Lamellar structures and self-replicating spots in a reaction-diffusion system

Kyoung J. Lee* and Harry L. Swinney
Center for Nonlinear Dynamics and the Department of Physics, The University of Texas, Austin, Texas 78712
(Received 3 June 1994)

Experiments on a ferrocyanide-iodate-sulfite reaction-diffusion system reveal several different planar spatial patterns: stationary lamellae arising from a transverse front instability and a front interaction; spot patterns that undergo a continuous process of growth through replication and death through overcrowding; waves with a repulsive front interaction; and conventional excitable waves that annihilate upon collision. The patterns form in a thin gel layer that is in contact with a continuously fed stirred reservoir. Lamellae are observed in both multistable and monostable regimes of the gel layer, while the self-replicating spots are found in a monostable regime. Numerical simulations on a one-dimensional, four-species model of the ferrocyanide-iodate-sulfite reaction describe the observed front interaction phenomena and some aspects of the bifurcation sequences observed in the laboratory experiments.

PACS number(s): 05.70.Ln, 82.40.Ck, 82.20.Mj, 82.20.Wt

I. INTRODUCTION

Many systems in nature and in technology develop spatial patterns when driven sufficiently far from thermodynamic equilibrium [1]. Patterns formed in chemical reaction-diffusion systems are a particularly interesting example because of the conjectured relation to patterns formed in biological systems [2]. Chemical patterns have been extensively discussed in theoretical biology [3–5], but until recently there were no laboratory studies of chemical patterns for sustained nonequilibrium conditions. Such studies become possible with the development of reactors in which patterns form inside a gel that has well-defined chemical concentrations imposed at the gel boundaries [6,7]. The gel prevents advective motion; thus the patterns that form arise from the interplay of reaction and diffusion processes. The system can be maintained indefinitely in a well-defined state by continuously refreshing the chemical reservoirs in contact with the gel boundaries, and the distance away from equilibrium can be controlled by varying the imposed concentration gradients.

Experiments using gel-filled reactors have revealed periodic and quasiperiodic rotating spiral patterns with an annihilating front interaction [8,9]; hexagonal, striped, and rhombic stationary (Turing) patterns [10–12]; waves and Turing spots in the vicinity of Turing and Hopf instabilities [13,14]; and patterns that are "turbulent" (irregular in both space and time) [15]. These experiments have all been conducted on just two chemical systems, the Belousov-Zhabotinsky (BZ) and the chlorite-iodide-malonic acid (CIMA) reactions.

The present study was undertaken to explore pattern formation in some chemical system other than the BZ and CIMA reactions. We chose a ferrocyanide-iodate-sulfite (FIS) reaction for the following reasons: (i) Like the BZ and CIMA reactions, the FIS reaction exhibits excitability, bistability, and oscillations in experiments in continuous flow stirred tank reactors [16]. (ii) Models have been developed for the kinetics of the FIS reaction [17–19]; hence a reaction-diffusion system with FIS kinetics can be numerically simulated and compared with observations. (iii) The FIS reaction in a stirred flow reactor exhibits large oscillations in pH [16]; hence any patterns that might form in an unstirred system could be visualized using a pH indicator.

Our experiments on the FIS reaction have revealed two types of patterns not found in previous studies: lamellae and replicating spots, as illustrated in Figs. 1(a) and 1(b), respectively. The lamellae develop through a transverse front instability: a perturbation of high pH in an initially spatially homogeneous low pH state evolves asymptotically into stationary irregular lamellae like that in Fig. 1(a); similar lamellar patterns form regardless of the shape of the initial perturbation [20]. This dynamic development of the pattern contrasts with small amplitude Turing patterns which form spontaneously at a bifurcation from the spatially uniform state [2,21–23]. The lamellae form for a wide range of reactor feed conditions, as long as the initial perturbation exceeds an amplitude threshold.

For another range of concentrations in the reactor feed, a dynamic pattern of self-replicating spots forms, as shown in Fig. 1(b) [24]. Like the lamellae, the spots must be initiated by a perturbation, but after initiation the spots grow and divide indefinitely. A newly formed spot will grow unless it is crowded by its neighbors, in which case it will die. The replicating spots and lamellar patterns both have short-range order but, unlike Turing patterns, no long-range order.

The wave fronts of the lamellae and replicating spots interact differently from those in the previously studied chemical patterns: as Fig. 1(c) illustrates, fronts ap-

*Present address: Department of Physics, Joseph Henry Laboratories, Princeton University, Princeton, NJ 08544.

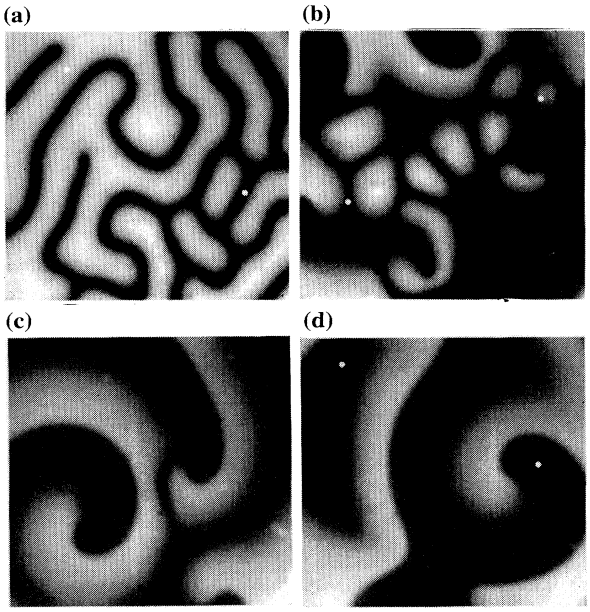

FIG. 1. Patterns observed in experiments with different ferrocyanide concentrations in the feed: (a) lamellae; (b) self-replicating spots; (c) spiral waves with wave front repulsion; (d) spiral waves with wave front annihilation. The patterns are illuminated in the blue (400–440 nm) and shown in full gray scale. The low pH state (roughly pH 4), which absorbs strongly in the blue, appears black, while the high pH state (roughly pH 7), appears white. The small white circles are end points of lines showing one-dimensional intensity profiles in Fig. 8. Each domain is 16×16 mm^2. The ferrocyanide concentrations in the feed are (in mM): $[K_4Fe(CN)_6 \cdot 3H_2O]_0 = 14.2$, 36.4, 30.0, and 25.0, respectively for (a)–(d). The concentrations of other reagents fed into the reservoir are held fixed (in mM): $[NaIO_3]_0 = 75.0$, $[Na_2SO_3]_0 = 89.0$, $[H_2SO_4]_0 = 3.6$, and $[NaOH]_0 = 0.25$, where the 0 subscript denotes values in the reservoir. The total input flow rate is 86.4 ml/h and the thickness of polyacrylamide gel is 0.4 mm.

proach and stop rather than collide and annihilate. This long-range inhibition is observed only in the regimes with lamellae and replicating spots. We also observe regimes with the type of front interaction that has long been studied in experiments on conventional excitable media such as the BZ reaction: fronts collide and annihilate, as Fig. 1(d) illustrates (the cusp in the upper right corner was formed by colliding fronts).

To gain some insight into the observed front interaction phenomenon, we have conducted numerical simulations of a one-dimensional reaction-diffusion model that uses a four-species kinetic scheme developed for the FIS system [19]. The one-dimensional model describes some aspects of the observed bifurcations, but of course cannot describe the two-dimensional features of pattern formation, such as the transverse front instability leading to lamellae.

Our experimental methods are described in Sec. II. The observations of lamellae are presented in Sec. III. Annular patterns and replicating spots are described in Sec. IV, which also describes lamellae that look similar to those in Sec. III but which have a different formation process—the lamellae in Sec. III can arise from either a uniform high or low pH state, while the lamellae in Sec. IV arise from a uniform low pH state. Section V compares results of numerical simulations of a one-dimensional model with the laboratory observations. Section VI compares the observed lamellae and replicating spots with results from several recent simulations of general two-dimensional reaction-diffusion models.

II. EXPERIMENTAL SYSTEM

A. Reactants

The ferrocyanide-iodide-sulfite system is an oscillating reaction developed by Edblom, Orbán, and Epstein [16]. The reaction is autocatalytic in iodide and the iodate-sulfite reaction is autocatalytic in both iodide and hydrogen ion. In our experiments the reactants are prepared in two groups that are not reactive separately. One group contains $NaIO_3$ (98+%, Aldrich), NaOH (Assay 98.0%, J. T. Baker Inc.), H_2SO_4 (Assay 98.0%, EM Science), and (when used) bromothymol blue pH indicator (ACS reagent, SIGMA). The other group contains Na_2SO_3 (98+% ACS reagent, Aldrich) and $K_4Fe(CN)_6 \cdot 3H_2O$ (ACS reagent, Aldrich).

The chemical solutions are prepared with doubly distilled water, and their concentrations are determined by the weights of the dissolved chemicals. The solutions are then filtered with cellulose nitrate membrane filters (pore size 0.45 μm, Micro Filtration Systems), degassed to prevent bubble formation in the reactor reservoir, and kept in a nitrogen atmosphere.

B. Reactor

Figure 2 is a schematic diagram of the gel reactor and optical system used in the present experiments [20]. Spatial patterns form in a thin transparent polyacrylamide hydrogel, which allows reaction and diffusion processes but prevents convection. Gel-filled reactors were developed several years ago to study spatial pattern formation in reaction-diffusion patterns maintained in well-defined states far from equilibrium [6,7] and have subsequently been used in many studies of spatial patterns in chemical systems.

The gel is made with a mixed monomer solution (5 ml of 16% acrylamide and 0.8% N,N'-methylene-bisacrylamide, both from Sigma), together with the initiator (80 μl of 30% triethanolamine and 80 μl of 20% ammonium persulfate, both from Sigma). The well-mixed solution is poured into a form on a glass plate and covered by a second glass plate; polymerization is completed within 10 min. The thickness of the gel membrane, determined by the spacing between the glass plates, is 0.2 or 0.4 mm [25]. The polymerized gel membrane is thoroughly washed with distilled water and cut for use in the experiments.

One side of the gel membrane is fed diffusively by

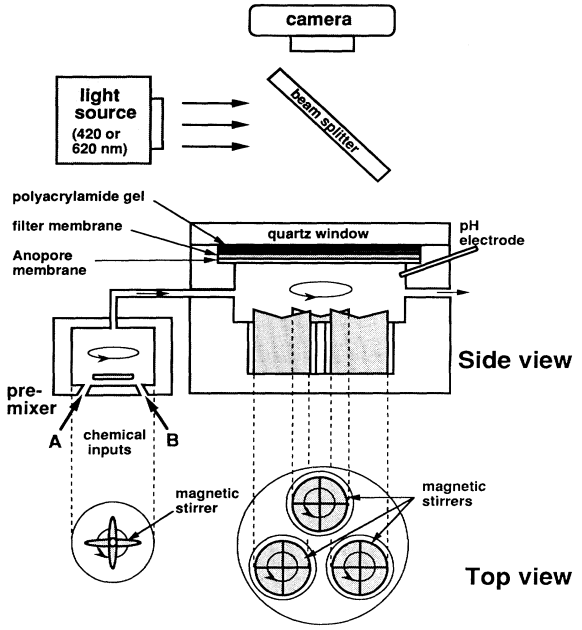

FIG. 2. Schematic diagram of the gel reactor and optical system. The reactor is drawn to scale except that the thicknesses of the gel membrane (0.2 mm), filter membrane, and Anopore membrane are four times larger than scale; the gel diameter is 22 mm. The premixer and main reservoir volumes are 0.5 and 2.5 ml, respectively.

a continuously refreshed stirred reservoir of chemicals. There are two thin membranes between this reservoir and the gel: an Anopore aluminum oxide disk (0.05 mm thick with 2-μm-diam pores), which provides structural rigidity for the gel layer, and a nitrocellulose membrane (0.14 mm thick with 0.45-μm-diam pores), which provides a white backing that improves visualization of the patterns (see Fig. 2). The other side of the gel membrane is in contact with a quartz window (25.4 mm diameter, 1.6 mm thick).

Each group of chemicals is pumped by a separate precision piston pump (Cheminert Metering Pumps, LDC/Milton Roy). Each pump has two small cylinders of 0.3 ml volume and two switching valves. The reagents are first fed to a vigorously stirred premixer and then to the main reservoir that feeds the gel membrane. Good mixing in the main reservoir is achieved using three magnetic stirring bars. The reservoirs and the whole reactor assembly are immersed in a temperature-controlled water bath (30 °C).

The pH of the reagents in the main reservoir is monitored with a resolution of 0.01 using a gel-filled pH electrode. The reservoir pH ranges from 7.0 to 7.5 for different experiments. In every case the pH is time independent, except for a small pulse [$\Delta(p\mathrm{H}) \simeq 0.01$] when the pump pistons and valves switch.

C. Visualization of patterns

The patterns are observed in backscattered light with the optical arrangement shown in Fig. 2. Absorption

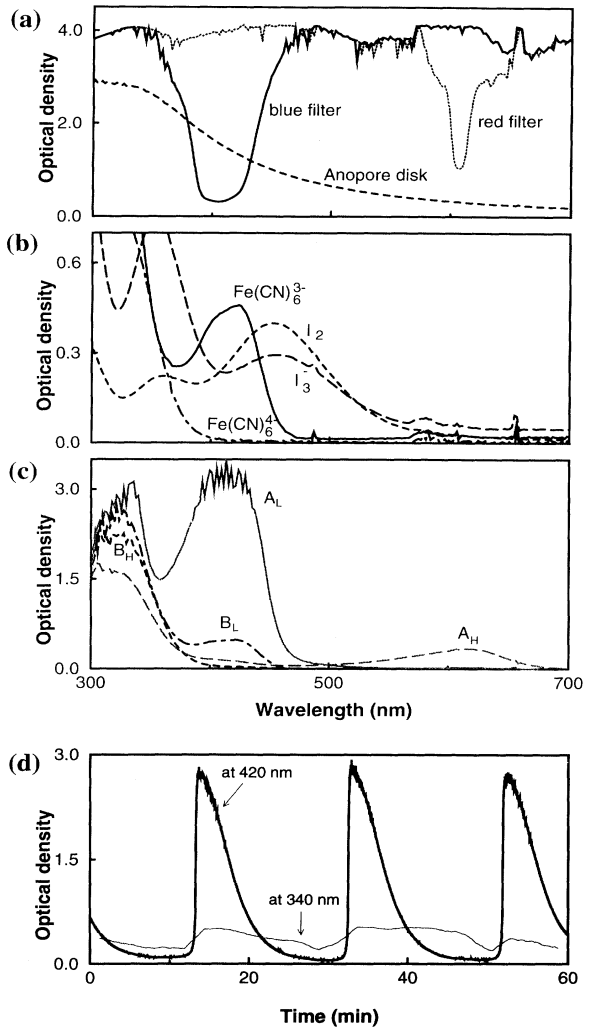

FIG. 3. Optical densities of (a) the Anopore aluminum oxide disk and the optical filters, (b) the major chemical species in the FIS reaction, (c) the FIS reaction in a stirred flow reactor in high pH and low pH states, as seen with bromothymol blue indicator (A_L, low pH; A_H, high pH) and without an indicator (B_L, B_H), and (d) the oscillating FIS reaction in a stirred flow reactor at 340 nm and 420 nm. The optical densities were determined with the following parameter values. In (a) sample thicknesses of Anopore (soaked in water before the measurement), red filter, and blue filters are, respectively, 0.05 mm, 5.0 mm, and 5.0 mm. In the measurements of (b) the optical path length is 0.18 mm; concentrations used are $[\mathrm{Fe(CN)_6}^{4-}] = [\mathrm{Fe(CN)_6}^{3-}] = 36.4$ mM, $[\mathrm{I_3}^-] = 18.75$ mM, and $[\mathrm{I_2}] = 8.93$ mM. In the measurements of (c): the optical path length is 9 mm; the input chemical concentrations are $[\mathrm{K_4Fe(CN)_6{\cdot}3H_2O}]_0 = 12.0$ mM, $[\mathrm{NaIO_3}]_0 = 75.0$ mM, $[\mathrm{Na_2SO_3}]_0 = 86.7$ mM, $[\mathrm{H_2SO_4}]_0 = 4.5$ mM, and $[\mathrm{NaOH}]_0 = 0.25$ mM; the volume of the reactor is 3 ml; the flow rate is 40 ml/h for the H states and 4 ml/h for the L states; the temperature is 25 °C. In the measurements of (d) the optical path length is 9 mm and the input chemical concentrations are $[\mathrm{K_4Fe(CN)_6{\cdot}3H_2O}]_0 = 25.0$ mM, $[\mathrm{NaIO_3}]_0 = 75.0$ mM, $[\mathrm{Na_2SO_3}]_0 = 89.3$ mM, $[\mathrm{H_2SO_4}]_0 = 4.5$ mM, and $[\mathrm{NaOH}]_0 = 0.25$ mM; the volume of the reactor is 3 ml and the flow rate is 10 ml/h; the temperature is 35 °C.

spectra for the optical components and the major chemical species in the reaction are shown in Figs. 3(a) and 3(b), respectively. Absorption spectra for the low and high pH states of the reaction are also shown in Fig. 3(c), which includes spectra for the reaction both with and without bromothymol blue indicator. Our early experiments used bromothymol blue indicator, and patterns were observed using red light. Then it was realized that the contrast is good even without an indicator if the patterns are observed in the blue where ferricyanide absorbs strongly [26]. Although tri-iodide and iodine also absorb in the blue, the absorption by tri-iodide and iodine is less than that of ferricyanide for the concentrations in our experiments [see Fig. 3(b)].

As can be seen in Fig. 4(c), there is a very large difference between the amount of absorption in the blue (380–440 nm) for the low and high pH states of the reaction. Figure 4(d) shows that the amplitude of the oscillations in absorption monitored at 420 nm, is much larger than at 340 nm, where the absorption is the same for ferrocyanide and ferricyanide [see Fig. 4(b)]; thus the observed patterns must arise primarily from absorption by ferricyanide rather than iodide, tri-iodide, or iodine.

Most of the measurements have been made without an indicator and with incident blue light. The patterns observed with and without the bromothymol blue indicator are essentially the same [20]. As Fig. 4 illustrates for the homogeneous reaction, the pH amplitude and the size of the hysteresis loop are very similar with and without bromothymol blue indicator.

In all figures, black represents low pH (roughly, pH 4) and white represents high pH (roughly, pH 7). Thus, to maintain throughout the paper the same convention of black for low pH and white for high pH, black and white have been reversed in the images obtained with bromothymol blue indicator (only Figs. 5 and 7) [27].

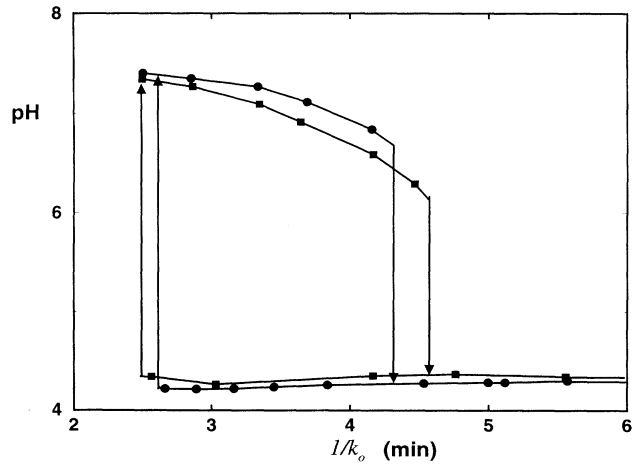

FIG. 4. Bistability in pH in a continuously fed stirred tank reactor experiment with (squares) and without (circles) bromothymol blue. Only k_0 (the inverse residence time) is changed with other parameters held fixed (all in mM): $[K_4Fe(CN)_6 \cdot 3H_2O]_0 = 12.0$, $[NaIO_3]_0 = 75.0$, $[Na_2SO_3]_0 = 86.7$, $[H_2SO_4]_0 = 4.5$, $[NaOH]_0 = 0.25$, and (when used) [bromothymol blue]$_0 = 0.026$.

The images are digitally acquired by a DAGE-MTI Nuvicon videocamera attached to a personal-computer-based frame grabber system. The signal-to-noise is improved by averaging ten images each 0.33 s; the image is then stored on a hard disk. Each image has a spatial resolution of 512×480 and each pixel has eight-bit resolution (the actual dynamic range is typically 50). The images are processed in a Silicon Graphics computer workstation.

D. Perturbation methods

The low intensity visible light used in the observations was found to have no discernible effect on either the patterned states or on the uniform low or high pH states. However, intense ultraviolet light does perturb the system, reducing ferricyanide to ferrocyanide (changing black regions to white). The stability of different spatial patterns was examined by illuminating the gel reactor with uv light in the desired pattern. Thus, for example, the stability of a pattern to perturbations of different wavelengths was studied by illuminating the reactor in the uv with stripes of different widths and spacings. The stability of the uniform low pH state was also studied using intense uv light as a perturbation.

The uniform high pH state could not be perturbed with light, but it was found that briefly stopping the stirring of the reservoir resulted in small, low pH regions in the uniform, high pH state.

III. LAMELLAE IN A MULTISTABLE REGIME

Experiments undertaken to examine the response of the FIS reaction-diffusion system to external perturbations revealed striking lamellar patterns, as shown in Fig. 5. For a wide range of reservoir concentrations, both low and high pH uniform states are stable in the gel. Spatial perturbations of either of these uniform states, as described in Sec. II D, evolve asymptotically to stationary lamellar patterns like that in the last frame ($t = 11$ h) in Fig. 5. In this particular example an initially uniform, high pH state in the gel was perturbed by stopping the stirring for 30 s; this resulted in the formation of a patch of the low pH state. Whatever the form of the perturbation, a transverse instability of the chemical front bounding the low pH region leads to the development of lamellae that are asymptotically stationary; the wavelength of the transverse instability is about 3 mm. Chemical fronts propagating towards one another slow down, reach a minimum separation, bounce back slightly, and then stop, as Fig. 6 illustrates. This type of strong front inhibition contrasts with the front annihilation behavior that has been studied in more than two decades of experiments and analyses of spirals and target waves in the Belousov-Zhabotinsky reaction [28].

The robustness of such irregular lamellae are demonstrated in Fig. 7: after a perturbation develops into stationary lamellae, that pattern is perturbed by irradiating

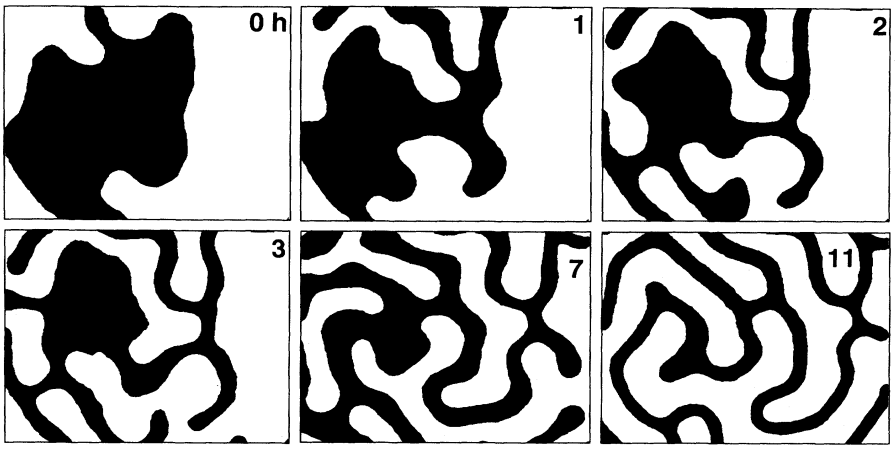

FIG. 5. Time development of lamellae from a perturbation of an initially homogeneous high pH state (white); the stirring in the reactor reservoir was stopped for 30 s to create a low pH domain (black). The patterns are observed with bromothymol blue indicator (0.15 mM) in reflected light of 620 nm. For consistency with the figures obtained without an indicator, regions observed as light and dark in the experiment have been reversed for the two figures obtained with the bromothymol blue indicator (this figure and Fig. 7); that is, the low pH state is shown as black and the high pH state as white [27]. The images are shown in a binary representation of the intensity for clarity. Each domain is 13×10 mm^2. The input chemical concentrations are $[K_4Fe(CN)_6 \cdot 3H_2O]_0 = 25.0$ mM; $[NaIO_3]_0 = 75.0$ mM; $[Na_2SO_3]_0 = 89.0$ mM; $[H_2SO_4]_0 = 4.5$ mM; and $[NaOH]_0 = 0.25$ mM. The total input flow rate F to the reactor is 124 ml/h and the thickness of the gel membrane is 0.2 mm.

a portion of the photosensitive system with intense uv light (254 nm) in parallel stripes. The imposed striped pattern is unstable and decays initially to the uniform high pH state, but soon thereafter irregular lamellae develop. The new lamellae are similar to, but not the same as, the original lamellae. Outside the perturbed region the pattern is essentially the same before and after the perturbation. Attempts to produce stable stationary regular patterns of parallel stripes failed: several striped perturbations with different line spacings and with varying total area were found to be unstable and evolved to irregular patterns like those shown in Figs. 5 and 7.

For clarity the lamellae in Fig. 5 are shown in a binary representation of the low and high pH states, but the fronts are not very sharp; hence in a binary representation the width of the high and low pH states depends to some degree on the choice of threshold. The gradual variation from low to high pH is apparent in Fig. 8, which shows the measured light intensity as a function of spatial position along different directions in Fig. 1. The length scales for the low and high pH lamellar bands are both typically 1 mm, but these length scales have a different dependence on control parameter, as Fig. 9 illustrates. The length scales are determined to an unknown degree by the thickness of the gel, which is 0.2 mm in Figs. 5–7 and 9 and 0.4 mm in Figs. 1 and 8.

The lamellae in this regime are observed to form only in response to a finite amplitude perturbation, in contrast to Turing patterns, which form spontaneously when a critical control parameter value is crossed. A perturbation below threshold values of width and amplitude decays

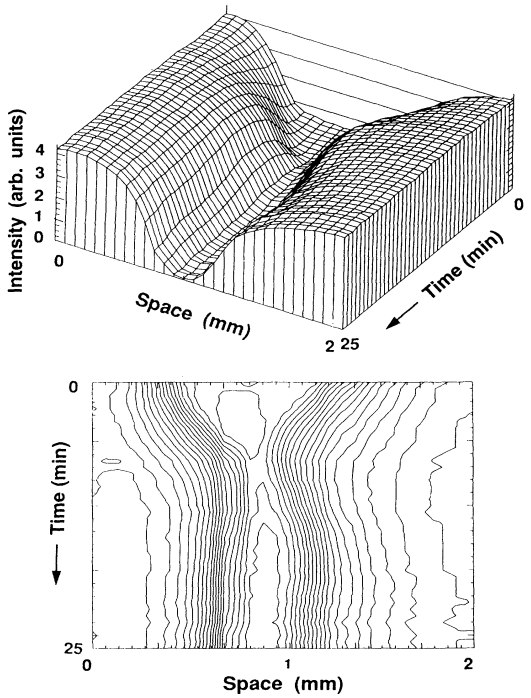

FIG. 6. Time evolution of two approaching chemical fronts (from a small region of Fig. 5). The upper graph shows the observed intensity as a function of space and time, where higher intensity corresponds to higher pH values. The corresponding contour plot (bottom) contains 20 equally spaced contour levels.

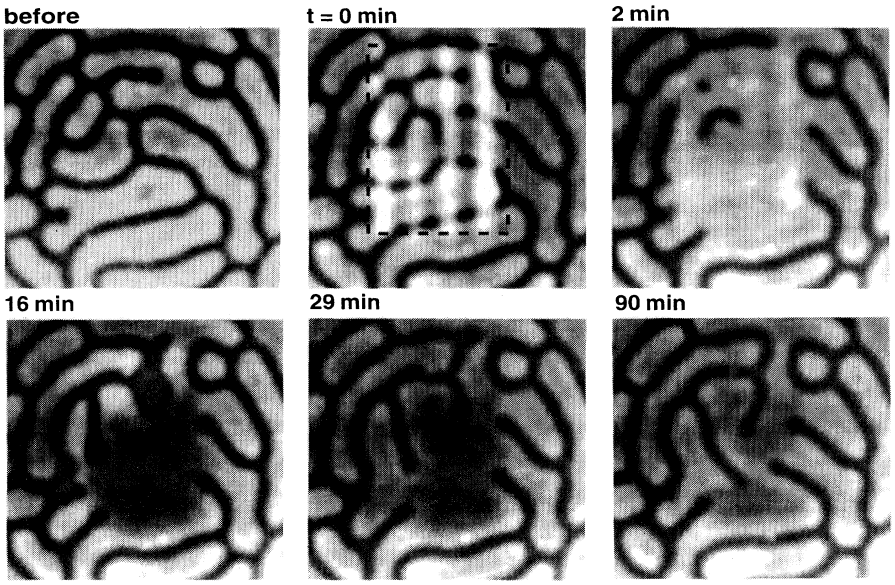

FIG. 7. Time evolution of lamellae following a perturbation with ultraviolet light. The perturbation is made with a striped mask for 5 minutes; only the boxed region bounded by dashed lines is perturbed. The perturbation is removed at $t = 0$. The patterns are observed with bromothymol blue indicator in reflected light of 620 nm (but note that black corresponds to low pH and white to high ph; see the caption to Fig. 5). Each frame is 13×13 mm^2. The parameter values are the same as given in the caption for Fig. 5.

to the homogeneous state, but a perturbation above the threshold width and amplitude evolves into a band whose shape is independent of the initial form of the perturbation. After a band achieves its final form, it can drift very slowly for hours until the whole system is filled with such bands, and then there is no further evolution of the pattern. The morphology of a final asymptotic state is always irregular, regardless of the initial perturbation; details of the final state depend of course on the history of the system such as the form of the initial perturbation and the rate of the parameter ramping.

The diagram in Fig. 10 shows the flow rate F values for transitions among lamellae and stable uniform states of low and high pH, and the range of their stability. If F is slowly increased, the system remains in the low pH state until there is a spontaneous transition to the uniform high pH state at $F = F_6$. Similarly, if the control parameter is slowly decreased from a large value, the system remains in the high pH state until there is a spontaneous transition to the uniform low pH state at $F = F_2$.

The parameter range in which patterns form was obtained by perturbing the homogeneous state with nonuniform uv light. The initial perturbations stabilize to patterns in the range $F_3 \leq F \leq F_4$; outside this range a perturbation decays to the homogeneous state. An example of time asymptotic stationary lamellae are shown in Fig. 5.

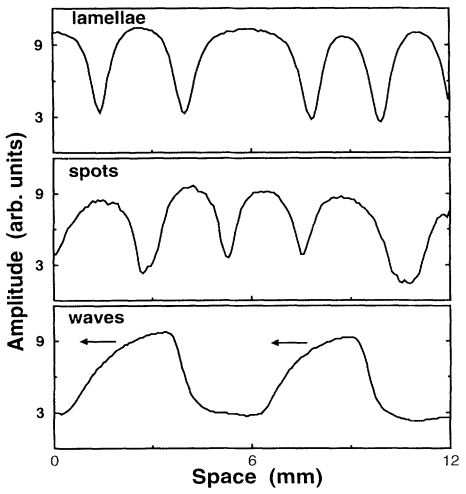

FIG. 8. Typical one-dimensional intensity profiles along lines connecting pairs of white dots in Fig. 1: lamellae from Fig. 1(a), spots from Fig. 1(b), and waves from Fig. 1(d).

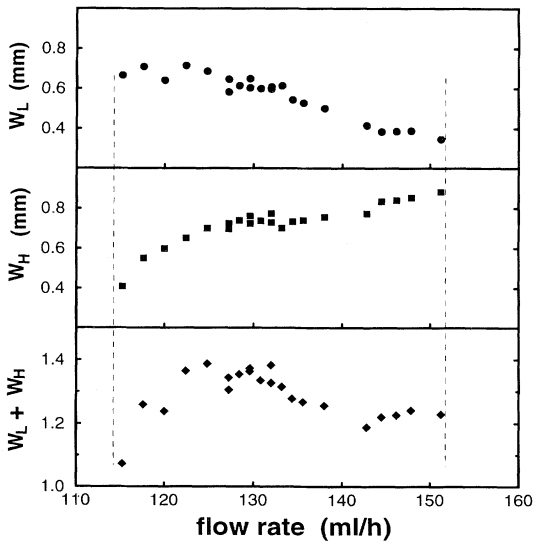

FIG. 9. Characteristic length scales W_L and W_H and their sum for low and high pH domains in experiment as functions of the total input flow rate. W_L (W_H) is obtained by dividing the area of the low (high) pH domain in a binary image such as Fig. 5 by one-half of the perimeter. Other parameters are held fixed as given in the caption for Fig. 5. The vertical dashed line on the left (right) marks the transition to the uniform low (high) pH state.

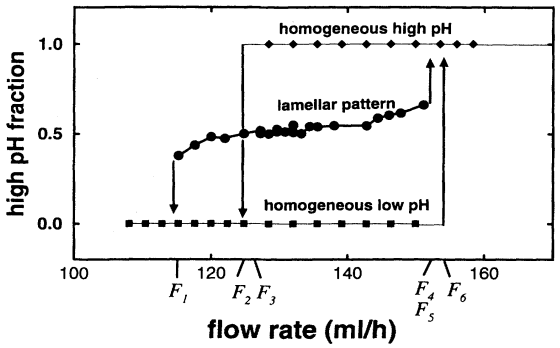

FIG. 10. Bifurcation diagram obtained in experiments showing transitions from the patterned state and to and from the uniform low pH and high pH states. The original patterns are binarized at an arbitrary cutoff value between the minimum and maximum gray values and the area ratio [(high pH area)/(total area)] is calculated. Only the flow rate F is varied. The values for F_1, F_2, F_3, F_4, F_5, and F_6 are 115, 125, 126, 152, 152, and 154 ml/h, respectively (see text). The other parameter values are held fixed as given in the caption for Fig. 5.

Once formed, lamellae persist throughout the range $F_1 \leq F \leq F_5$, although with each change in F within this range, the pattern changes its wavelength and morphology. The lamellar state is an attractor in the sense that the fraction of the total area in the high pH state (see Fig. 10) approaches the *same* value after a pattern is perturbed for a period of time in any of the following ways: (i) illumination of the pattern with intense uv light (as in Fig. 7); (ii) stopping the stirring of the reservoir; (iii) decreasing the flow rate to some smaller value in the range $F_1 \leq F \leq F_5$ and then later returning the flow rate to its original value; and (iv) increasing the flow rate to some larger value in the range $F_1 \leq F \leq F_5$ and then later returning the flow rate to its original value. Thus, although the details of a lamellar structure depend on the initial conditions and the parameter ramping, the lamellar state is robust and nonhysteretic.

IV. SPOTS, ANNULI, REPULSIVE WAVES, AND LAMELLAE

Several unusual patterns are observed in experiments conducted with lower pH and lower flow rates than those used in the experiments in the preceding section. Only a single, stable uniform state, the low pH state, is stable for the parameter values used in the experiments described in this section. The bifurcation parameter is the ferrocyanide concentration in the reservoir feed; all other parameters are held fixed at the values given in Fig. 11.

A. Self-replicating spots and annuli

Self-replication of spots of high pH in a background of low pH is illustrated in Fig. 11(a). In an initially homogeneous medium of low pH, spots can be initiated with a finite amplitude perturbation (with uv light or by briefly stopping the stirring of the reservoir or by an inhomogeneity at the gel boundary). Small amplitude perturbations decay. Once initiated, the spots are self-sustaining. A spot grows and then divides into smaller spots. A newly formed spot initially shrinks and will die if it is crowded by neighboring spots, but if it is not too crowded, it shrinks only slightly before it begins to grow. The minimum diameter of an isolated spot is about 1.2 mm for the conditions of Fig. 11. The growth process is strongly affected by interaction with neighboring spots. Spots squeeze one another but never collide. Consequently, neighboring spots elongate in the direction perpendicular to a line between their centers. Each elongated spot eventually pinches off and divides into two smaller daughter spots. Occasionally a spot crowded by several neighbors will divide into three or more spots, but division into two spots is much more common.

An isolated spot will grow into an annulus rather than dividing into two spots. Such an isolated spot occasionally emerges in a region that was so crowded with spots that most of them died, leaving a uniform low pH background with a single spot of high pH. The isolated spot grows until the diffusive feed of reagents through the boundary of the spot and from the reservoir is no longer sufficient to maintain the center in the high pH state. Then the pH in the spot center drops, leaving an annulus, as shown in Fig. 11(b) and in the corresponding sequence of intensity profiles in Fig. 12. This sequence looks similar to that for a pacemaker in an excitable medium, but in contrast to the usual pacemakers, which are fixed in space, each successive cycle here occurs at a different location. Moreover, unlike conventional waves in excitable media, which have a steep front and a long refractory tail, the tail of the growing ring is steeper than the front. As the ring grows, the steepness of the leading and trailing edges becomes comparable and the propagation stops. The maximum outer diameter of the annulus structure is about 9 mm.

An annulus deforms through interactions with neighboring spots and eventually the annulus breaks into several pieces. These pieces and other structures (spots and remnants of other annuli) continuously grow and divide, giving rise to a complex spatiotemporal pattern with no discernible long-range order in space or time.

B. Wave repulsion

When the input ferrocyanide concentration in the experiment is decreased, there is a transition at a critical concentration to a regime without replicating spots, but traveling waves still repel one another, as Fig. 13 illustrates. A channel develops between two approaching fronts, just as in the replicating spot regime, but now the low pH channel invades and breaks the high pH front, as can be seen in Fig. 13 at $t = 8$ min. This process leads to a highly irregular global pattern with no well-defined length scale. This contrasts with the locally ordered spiral and target patterns of excitable media [28], where waves collide and annihilate. Moreover, in con-

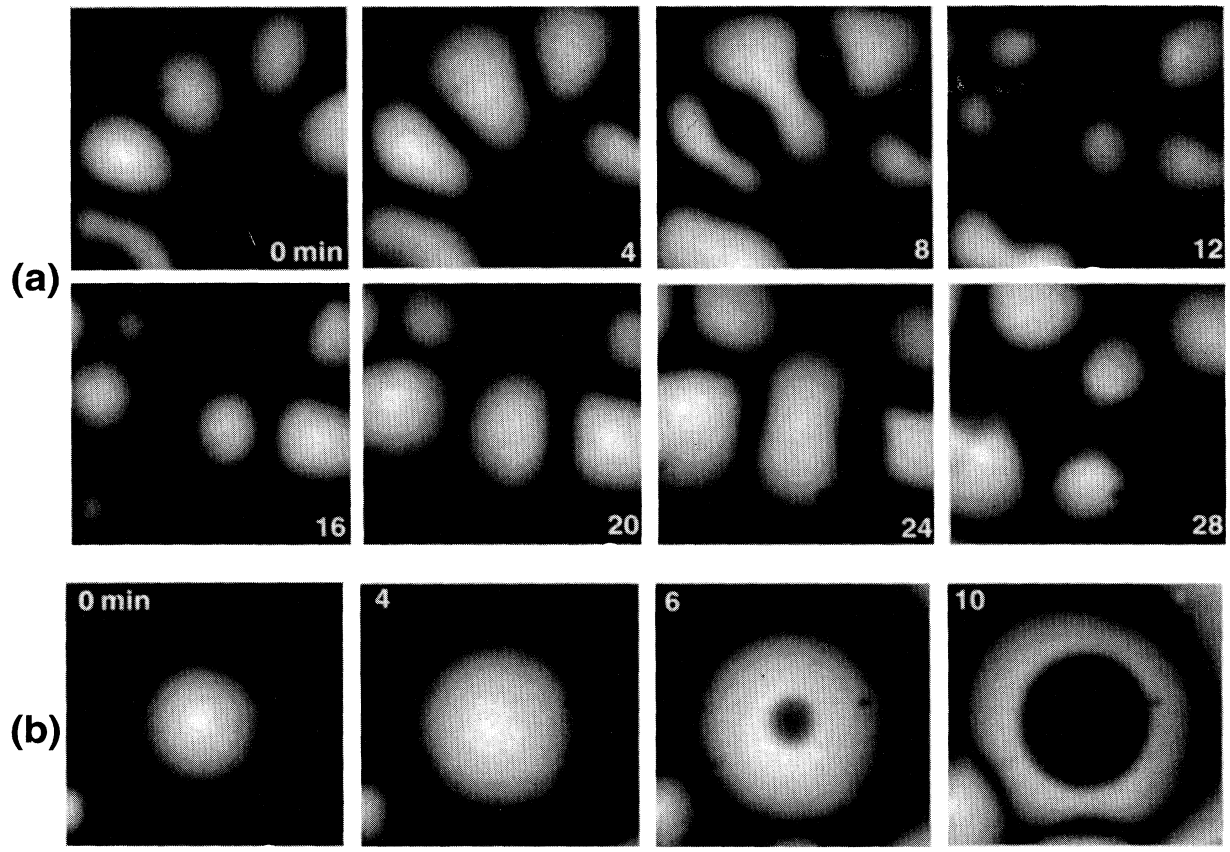

FIG. 11. Experimental observations of (a) self-replicating spots and (b) formation of a ring. In (a), chemical spots (white; high pH) undergo two successive divisions. The divisions are strongly influenced by neighboring spots. Each frame is 7×7 mm^2. In (b), an isolated spot of high pH state grows until its center collapses into the low pH state. The ring eventually interacts with neighboring structures and breaks. Each frame is 10×10 mm^2. Both (a) and (b) are observed with illumination at 420 nm in a system without bromothymol blue indicator. Both phenomena are observed with following parameter values: $[K_4Fe(CN)_6 \cdot 3H_2O]_0 = 36.4$ mM, $[NaIO_3]_0 = 75.0$ mM, $[Na_2SO_3]_0 = 89.0$ mM, $[H_2SO_4]_0 = 3.6$ mM, and $[NaOH]_0 = 0.25$ mM. The total input flow rate is 86.4 ml/h and the thickness of the gel membrane is 0.4 mm.

ventional excitable media, waves die at a wall, while the present waves are reflected by a wall, as Fig. 14 illustrates. Refraction and reflection of chemical waves have been observed at an interface between two gels [29], but the reflection from a rigid wall has not been previously reported.

C. Transition to a stationary lamellar pattern

When the input ferrocyanide concentration is decreased from the regime described in the preceding subsection, the first transition reached is to a state with waves that collide and annihilate, as in conventional excitable media; see Fig. 1(d). A further reduction in ferrocyanide concentration in the feed leads to a second transition, to a regime in which lamellae dynamically develop, as Fig. 15 illustrates. No finite amplitude perturbation is required to initiate these patterns, in contrast to the lamellae described in Sec. III. The lamellae grow quite rapidly, sometimes from several directions: low pH domains, which are random in size and shape, occasionally emerge spontaneously from a high pH background and form filaments as they collapse. After the low pH filaments fill the domain, they slowly rearrange and adjust in width to achieve an asymptotic stationary pattern, like that in the final frame in Fig. 15 ($t = 40$ min). The final pattern in Fig. 15, like the one in Fig. 5, is irregular, but the growth processes leading to the final patterns differ; for example, in Fig. 15 the low pH fronts sometimes meet and connect (two of the three filaments that end on the left side of $t = 0$ image connect by $t = 16$ min). In contrast, in the previously described lamellae, low pH fronts approach and stop, as discussed in Sec. III.

D. Transition to a homogeneous state

The final state reached with low input ferrocyanide concentration is homogeneous low pH. The transition from the patterned to a homogeneous state is shown in Fig. 16. The patterns disappear not by decreasing the thickness but by shrinking in length.

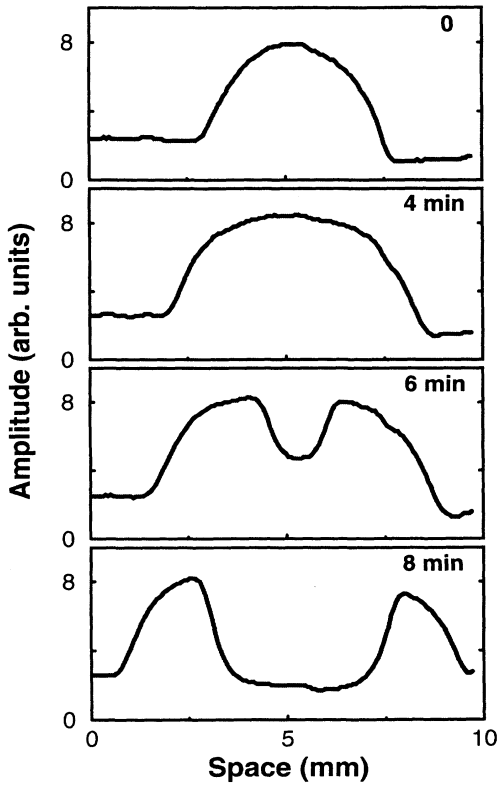

FIG. 12. Intensity profiles showing the formation of an annulus. The graphs correspond to the snapshots in Fig. 11(b).

V. NUMERICAL SIMULATIONS IN A MODEL

We have examined the front inhibition phenomenon in a one-dimensional, four-species model of the FIS reaction. Patterns in the experiments of course form in a three-dimensional gel, but the characteristic length scales of these patterns are comparable to or larger than the gel thickness; hence the reduction from three to two dimensions is a reasonable approximation. However, the further reduction to one dimension means that our model cannot describe the transverse front instability problem. We had hoped to examine this instability, but our computer resources were inadequate for simulating the stiff FIS kinetics in two dimensions. As we will describe in Sec. VI, recent simulations by other researchers of two-species models with cubic kinetics have yielded lamellar patterns similar to those we have observed.

TABLE I. Values of rate constants in the FIS model in Sec. V A (from Ref. [19]).

Rate constants	Values
k_1	$5.0 \times 10^{10}\ M^{-1}\mathrm{s}^{-1}$
k_{-1}	$8.1 \times 10^{3}\ \mathrm{s}^{-1}$
k_2	$8.0 \times 10^{-1} \times [IO_3^-]_0\ M^{-1}\mathrm{s}^{-1}$
k_3	$1.0 \times 10^{6} \times [IO_3^-]_0\ M^{-2}\mathrm{s}^{-1}$
k_4	$2.3 \times 10^{9}\ M^{-1}\mathrm{s}^{-1}$
k_5	$1.2 \times 10^{3} \times [Fe(CN)_6^{-4}]_0\ M^{-1}\mathrm{s}^{-1}$

A. Four-species FIS reaction-diffusion model

The FIS reaction involves several component processes that have a long history in chemical kinetics. Building on previous work on the component reactions, Edblom *et al.* developed a kinetic model with 12 species [17]. Gáspár and Showalter independently developed a similar but ten-species model of the FIS reaction [18,19]. Gáspár and Showalter also showed that a reduced four-species model provides a qualitative description of the experiments on the FIS reaction in a continuous flow stirred tank reactor.

The variables in the four-species Gáspár-Showalter model are $A \equiv SO_3^{2-}$, $X \equiv HSO_3^-$, $Y \equiv H^+$, and $Z \equiv I_2$. The model is as follows:

$$A + Y \overset{k_1, k_{-1}}{\rightleftarrows} X,$$
$$X \overset{k_2}{\rightarrow} Y,$$
$$2Y \overset{k_3}{\rightarrow} Z,$$
$$Z + X \overset{k_4}{\rightarrow} 3Y,$$
$$Z \overset{k_5}{\rightarrow} .$$

The rate constants k_i are given in Table I. The other input species IO_3^- and $Fe(CN)_6^{-4}$ are assumed to be in excess and hence to vary little in the course of the reaction; their values are incorporated in the rate constants. The four-species model is similar to the autocatalator proposed by Gray and Scott [30] and also discussed by Peng *et al.* [31].

Even the ten-species model has some deficiencies; e.g., Luo and Epstein have proposed that the direct reaction between iodate and ferrocyanide plays an essential role in the oscillatory reactions as a negative feedback process [32], while Gáspár and Showalter's ten-species model does not include the process. For simplicity we use the Gáspár-Showalter's four-species model in our numerical simulations of a one-dimensional reaction-diffusion system.

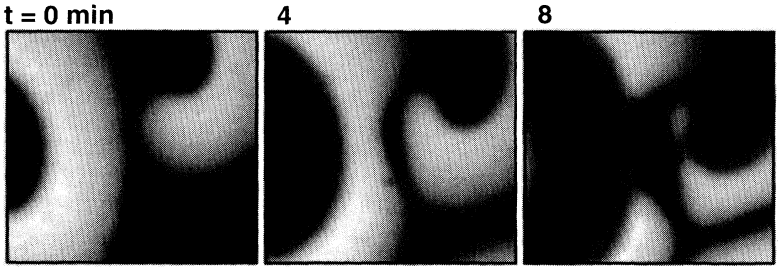

FIG. 13. Snapshots showing a repulsive chemical front interaction. The patterns are observed in illumination at 420 nm without bromothymol blue indicator. The domain is 8.2 × 8.2 mm^2. The parameter values are the same as given in the caption for Fig. 11, except $[K_4Fe(CN)_6 \cdot 3H_2O]_0 = 30.0$ mM.

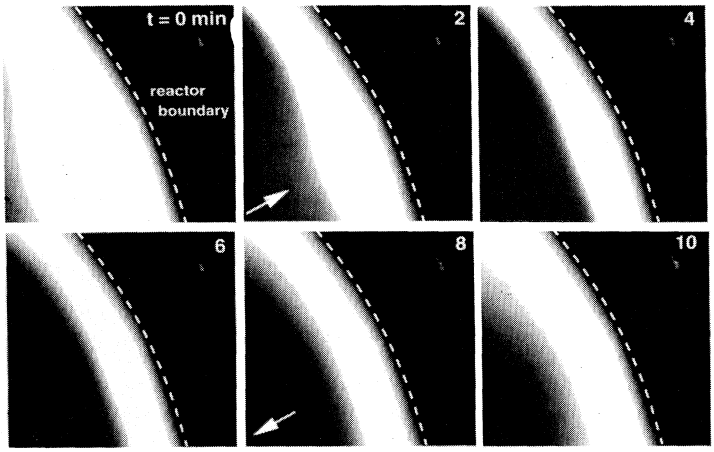

FIG. 14. Snapshots showing observations of an excitable wave reflecting from the reactor boundary. The patterns are observed in illumination at 420 nm without bromothymol blue indicator. The domain is 5.2×5.2 mm^2. The parameter values are the same as given in the caption for Fig. 13.

Our one-dimensional reaction-diffusion model with the four-species FIS kinetics is

$$\begin{aligned}
\partial X/\partial t &= D_X \partial^2 X/\partial x^2 + k_1 AY - k_{-1}X \\
&\quad -k_2 X - k_4 ZX - k_0 X, \\
\partial Y/\partial t &= D_Y \partial^2 Y/\partial x^2 - k_1 AY + k_{-1}X \\
&\quad +k_2 X - 2k_3 Y^2 + 3k_4 ZX + k_0(Y_0 - Y), \\
\partial Z/\partial t &= D_Z \partial^2 Z/\partial x^2 + k_3 Y^2 - k_4 ZX - k_5 Z - k_0 Z, \\
\partial A/\partial t &= D_A \partial^2 A/\partial x^2 - k_1 AY + k_{-1}X + k_0(A_0 - A),
\end{aligned}$$

where the D's are diffusion coefficients and the terms involving the inverse residence time (k_0) model flux exchanges between the gel membrane and the reservoir [33]. The chemical concentrations ($[\text{conc}]_0$) used in the numerical simulations are given in the figure captions. The diffusion coefficient values used are $D_Y = D_Z = D_A = 1.0 \times 10^{-5}$ cm^2/s and $D_X = 2.0 \times 10^{-5}$ cm^2/s. Simulations conducted with D_X values down to 1.3×10^{-5} cm^2/s yielded qualitatively similar patterns, but when D_X was smaller than 1.3×10^{-5} cm^2/s, no stationary pattern and no replicating spots were found. A few runs made with $D_X = D_Z = D_A = 1.0 \times 10^{-5}$ cm^2/s, and $D_Y = 2.0 \times 10^{-5}$ cm^2/s (with other parameter values fixed as before) yielded no interesting patterns, except transient simple fronts.

The second-order spatial derivatives are discretized by a finite difference method and the resulting ordinary differential equations are solved by a stiff differential equation solver which uses a backward Gear scheme [34]. A fine spatial mesh ($\delta x = 5.0 \times 10^{-3}$ mm) with time steps $\delta t \leq 0.1$ s is used to ensure convergence of the solution. No flux boundary conditions are used at both ends of the spatial grid. The spatial grid of 3200 points covers 16 mm in real space, which is enough to contain several wavelengths of the pattern. A few runs made with 1600 or 6400 grid points yielded qualitatively similar patterns.

B. Front interaction in the FIS model

The interaction of fronts generated by a local high pH perturbation of a homogeneous low pH state is illustrated

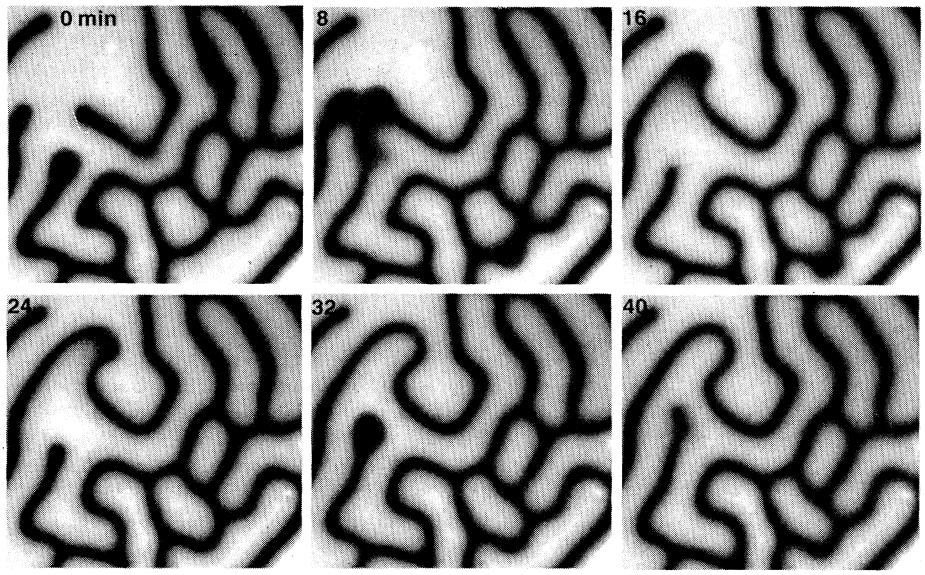

FIG. 15. Snapshots of a pattern evolving to a stationary pattern of low pH lamellae in a high pH background. Unlike the lamellar pattern in a bistable regime (Fig. 5), the fronts sometimes collide and annihilate. The patterns are observed in illumination at 420 nm without bromothymol blue indicator. The domain is 16×16 mm^2. The parameter values are the same as given in the caption for Fig. 11, except $[K_4Fe(CN)_6 \cdot 3H_2O]_0 = 14.2$ mM.

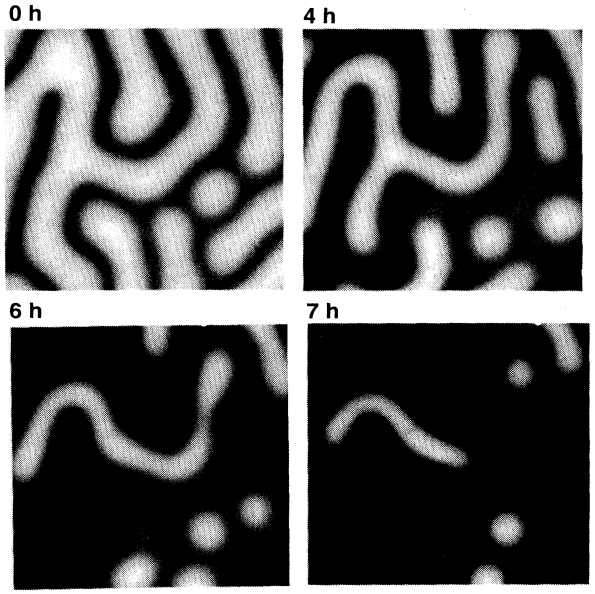

FIG. 16. Transition from a lamellar pattern to the homogeneous low pH state, observed following a decrease in $[K_4Fe(CN)_6 \cdot 3H_2O]_0$ from 14.2 mM to 13.0 mM at $t = 0$. The high pH stripes disappear more by shrinking in length than by decreasing in thickness. The patterns are observed in illumination at 420 nm without bromothymol blue indicator. The domain is 13 × 13 mm^2. Other parameter values are held fixed as given in Fig. 11.

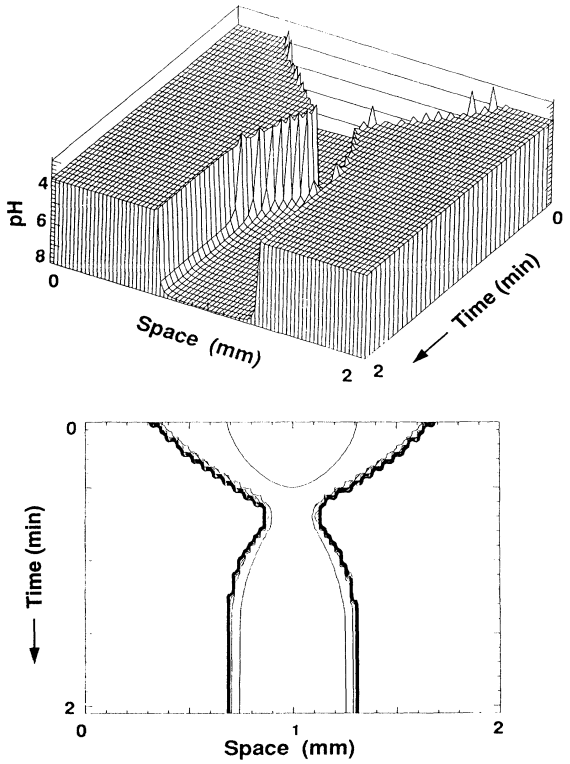

FIG. 17. Time evolution of two approaching chemical fronts in a simulation on a one-dimensional four-species FIS reaction-diffusion model. The graph in the top is a pH space-time diagram and the graph below is the corresponding two-dimensional contour plot with 20 equally spaced contour levels; compare the similar behavior observed in the experiment, shown in Fig. 6. The parameter values in the simulation are $[Fe(CN)_6^{-4}]_0 = 2.0$ mM, $[IO_3^-]_0 = 75.0$ mM, $[SO_3^{-2}]_0 = 89.3$ mM, $[H^+]_0 = 9.0$ mM, and $k_0 = 0.014$ s^{-1}. $[Fe(CN)_6^{-4}]_0$ in the simulation is 12.5 times smaller than in the experiment; no patterns were found in the simulations for the laboratory values of concentrations that yielded patterns.

in Fig. 17. [In this regime, homogeneous states with low pH (about 4) and high pH (about 8) are both stable.] When the resulting chemical fronts approach close, they repel and then stabilize in an essentially stationary band structure. As in the experiment, only a perturbation above a threshold width and amplitude evolves into a band structure whose shape is independent of the initial form of the perturbation.

The structure shown in Fig. 6 (experiment) is a low pH band, while the structure in Fig. 17 (simulation) is a high pH band. When a low pH band is used as an initial perturbation of the homogeneous high pH state in the simulation, the two fronts first approach one another, repel, and then move away to the boundary, as shown in Fig. 18(a). However, in simulations in a monostable regime we found stable low pH bands, just as found in the experiment, as Fig. 18(b) illustrates. The fronts that connect the high and low pH domains are much steeper in the simulation than in the experiment; compare the fronts in Fig. 17 with those in Fig. 6.

A bifurcation diagram obtained by varying k_0 in the simulation (Fig. 19) can be compared to the diagram obtained by varying F in the experiment (Fig. 10). If k_0 is slowly increased, the system remains in the low pH state until there is a spontaneous transition to the uniform high pH state at $k_0 = k_{06}$. Similarly, if the control parameter is slowly decreased from a large value, the system remains in the high pH state until there is a spontaneous transition to the uniform low pH state at $k_0 = k_{02}$.

The parameter range in which patterns form were obtained by perturbing the homogeneous state with a spatially periodic square wave (2 mm wavelength). The initial perturbations stabilize to patterns (see Fig. 20) in the range $k_{03} \leq k_0 \leq k_{04}$; outside this range a perturbation decays to the homogeneous state, as in the experiments. Presumably the final length scales are determined by the chemical kinetics and the diffusion coefficients of the chemical species. A similar stable structure was found by Hagberg and Meron in a study of a one-dimensional FitzHugh-Nagumo model, and they showed that the length scale was given in terms of the chemical kinetics and diffusion coefficients [35].

Once formed, the stationary periodic structure persists throughout the range $k_{01} \leq k \leq k_{05}$, as in the experiment; with each change in k_0 within this range, the initial banded pattern evolves to another banded pattern with a different characteristic length scale. The subcritical transitions between the patterned and homogeneous states are similar in the experiment and simulation. In

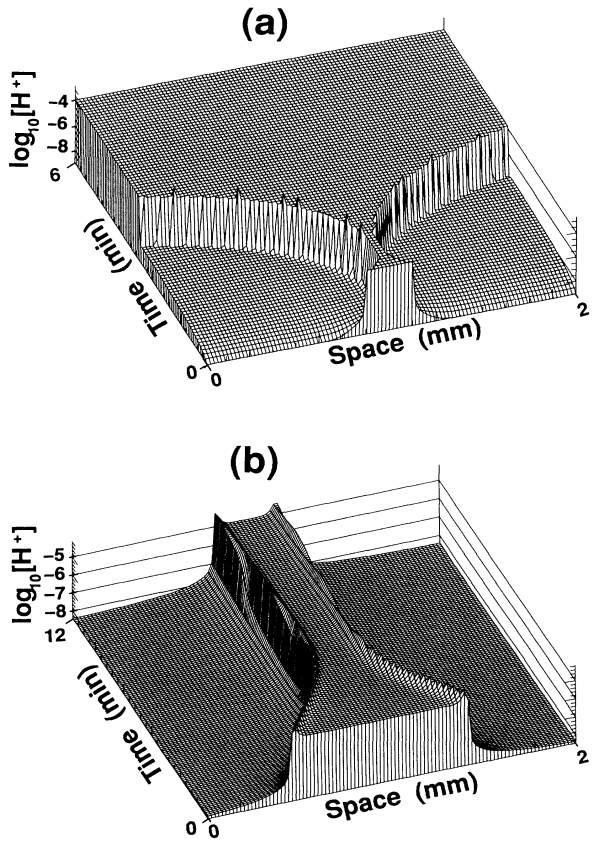

FIG. 18. Perturbations of initially uniform states of high pH in the simulations: (a) fronts repel and propagate to the boundaries; (b) fronts interact and stabilize into a low pH pulse. The parameter values in (a) are $[Fe(CN)_6{}^{-4}]_0 = 2.0$ mM, $[IO_3{}^-]_0 = 75.0$ mM, $[SO_3{}^{-2}]_0 = 89.3$ mM, $[H^+]_0 = 9.0$ mM, and $k_0 = 0.02$ s^{-1}. The corresponding parameter values in (b) are 0.01 mM, 75.0 mM, 89.3 mM, 1.0 mM, and 1.0×10^{-4} s^{-1}.

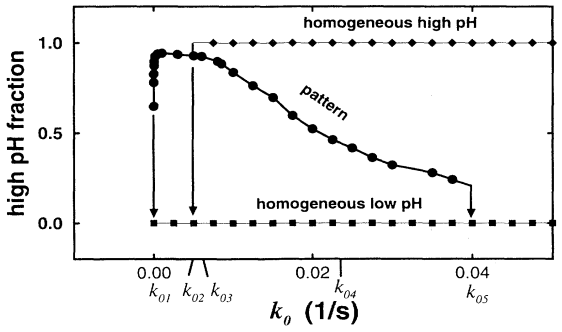

FIG. 19. Bifurcation diagram obtained in a numerical simulation of a one-dimensional FIS reaction-diffusion model, showing transitions to and from the patterned state and to and from the uniform low pH and high pH states. The original patterns are binarized with a cutoff value of pH 5.7. Only k_0 is varied. The values for k_{01}, k_{02}, k_{03}, k_{04}, k_{05}, and k_{06} are 2.0×10^{-6}, 5.0×10^{-3}, 6.0×10^{-3}, 23.0×10^{-3}, 40.0×10^{-3}, and 62.3 s^{-1} (beyond the range shown), respectively. Other parameter values are fixed as given in the caption for Fig. 17.

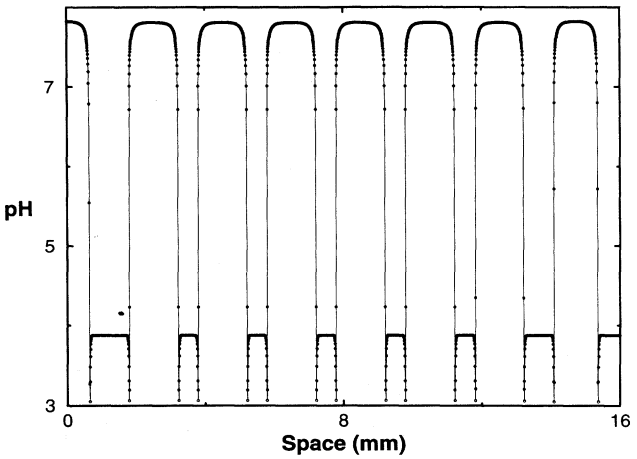

FIG. 20. A time asymptotic stationary pattern obtained in the simulation with $k_0 = 0.02$ s^{-1}. Other parameter values are the same as given in the caption for Fig. 17. The narrow peaks near pH 3 here and in Figs. 17 and 18 are fully resolved; they are essentially unchanged when a finer spatial mesh is used.

both experiment and simulation there is no hysteresis in the high pH fraction with increasing and decreasing control parameters. However, in the experiment the high pH fraction increases with increasing F, while the high pH fraction decreases with increasing k_0 in the simulation.

C. Replicating spots and other patterns in the FIS model

The observed spot replication and wave repulsion phenomena (see Sec. IV) are described well by the model in a regime with monostable kinetics. The bifurcation parameter in the experiments was the ferrocyanide concentration in the reservoir feed. Ferrocyanide does not appear explicitly in the model but is contained in the rate constant k_5 (see Sec. V A). The experiments show that increasing either $[H^+]_0$, a parameter that is explicit in the model, or the ferrocyanide concentration in the feed has a similar affect on the patterns; therefore, in the simulations we choose $[H^+]_0$ as the control parameter.

The one dimensional numerical simulations reveal replicating behavior similar to that observed in experiment (see Fig. 11), as illustrated in Fig. 21(a), which shows the post-transient time evolution of a pattern initiated by perturbing a homogeneous low pH domain with a single, high pH, finite amplitude spot. (In one dimension there is no distinction between spot division and the development of an annulus.) Small amplitude perturbations decay, as in the experiment.

The spot division mechanism in one dimension is illustrated by the small region bounded by dashed lines in Fig. 21(a); profiles of pH as a function of position are shown in Fig. 22 for four times during the process of spot division. Spots smaller than about 0.4 mm die; a spot larger than the minimum size will grow if it has no near neighbors, but will die if it is overcrowded. An isolated

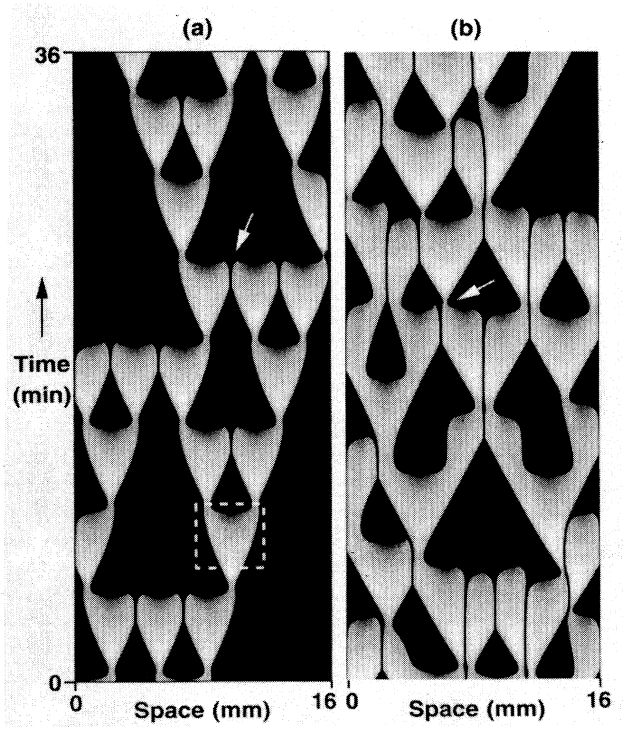

FIG. 21. Numerical simulations of (a) one-dimensional replicating spots and (b) excitable waves with front repulsions. Both space-time diagrams show asymptotic behavior after initial transients have decayed. A small domain of high pH (pH 8; white) is seeded initially as a perturbation of a homogeneous low pH (pH 3; black) state (not shown in the figure) and subsequent time evolution is integrated. In (b) the interaction of fronts and the reflection from walls are similar to that in the laboratory observations shown in Figs. 13 and 14. The parameter values used in (a) are $[Fe(CN)_6{}^{-4}]_0 = 2.5$ mM, $[IO_3{}^-]_0 = 75.0$ mM, $[H^+]_0 = 12.5$ mM, $[SO_3{}^{-2}]_0 = 89.3$ mM, and $k_0 = 1.0 \times 10^{-4}$ s^{-1}. The parameter values for (b) are the same as in (a), except that $[H^+]_0 = 11.0$ mM.

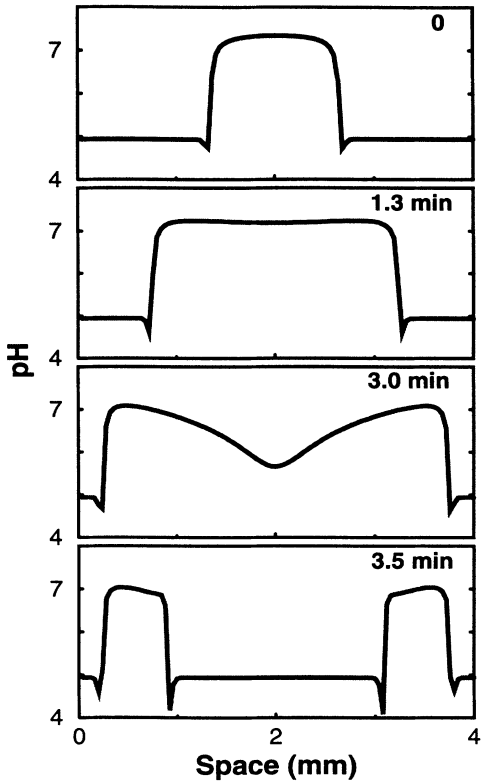

FIG. 22. Profiles of pH showing spot replication in the simulation, which can be compared with the experimental results shown in Fig. 12. The graphs in the time sequence are obtained from the boxed region in Fig. 21(a).

spot grows to about 3.4 mm in size. Then the diffusive flux through the boundaries and from the reservoir is no longer sufficient to maintain the center in the high pH state and the center collapses to the low pH state, leaving two spots. After division, the leading and trailing edges develop a similar steepness, just as in the experiment, although the fronts are much steeper in the simulation than in the experiment. The spatiotemporal behavior in the experiment and simulation is similar: locally the behavior is simple and deterministic, while globally the system has no long-range spatial or temporal order.

The wave repulsion phenomenon observed in the experiments is also captured by the simulations when $[H^+]_0$ is decreased from the range yielding replicating spots. Interacting chemical fronts in the model form channels—the long black vertical lines in Fig. 21(b). As in the laboratory experiment (see Fig. 13), the channel structures are transient and waves reflect from the boundaries. A refractory tail oscillates toward and away from its front, which propagates at almost constant speed until it interacts with other fronts. In the replicating spot regime adjacent spots always decay [see the arrow in Fig. 21(a)], while in this regime one or both persist [see the arrow in Fig. 21(b)].

The transitions found in the model with decreasing $[H^+]_0$ have similarities to those observed in the experiments with decreasing ferrocyanide concentration in the feed. The space-time diagram in Fig. 23(a) shows how low pH regions interact and evolve to a stationary spatially periodic state: low pH spots spontaneously emerge and annihilate, adjusting in spatial density and oscillating in their separation until the final state is achieved. This breathing behavior can also be seen when the direction in which $[H^+]_0$ is reversed, as Fig. 23(b) illustrates.

The final state reached with decreasing $[H^+]_0$ is homogeneous with high pH, while the final state reached in the experiment is homogeneous with low pH. Simulations with small steps in $[H^+]_0$ reveal, between the regime with periodic structure (Fig. 23) and the homogeneous state, an irregularly oscillating pattern with occasional "firings" of low pH, as shown in Fig. 24. This continuously evolving pattern forms when the homogeneous kinetics is in the oscillatory regime. Such a pattern has not been found in previous experiments or simulations, although oscillating domains with different modes have been studied in model systems [35,36]. Future experiments could use a

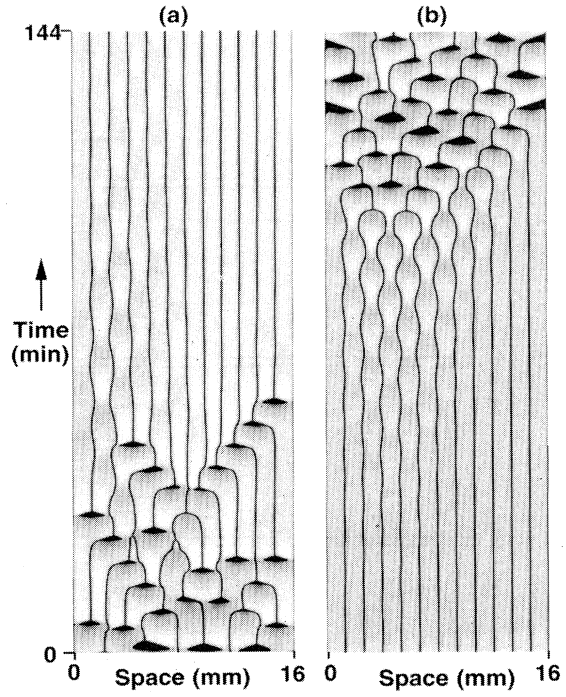

FIG. 23. (a) Space-time evolution showing formation of a stationary periodic structure in numerical simulation, after $[H^+]_0$ is decreased from 8.5 mM, where waves repel and there is no asymptotic stationary pattern, to $[H^+]_0 = 7.5$ mM, where the pattern stabilizes in a stationary spatially periodic structure. The transient behavior, although one dimensional, has similarities to that observed in experiments on two-dimensional patterns (Fig. 15). (b) Destabilization of a stationary structure. $[H^+]_0$ is increased from 7.5 mM to 8.5 mM at $t = 0$. Other parameter values are held fixed as given in the caption for Fig. 21.

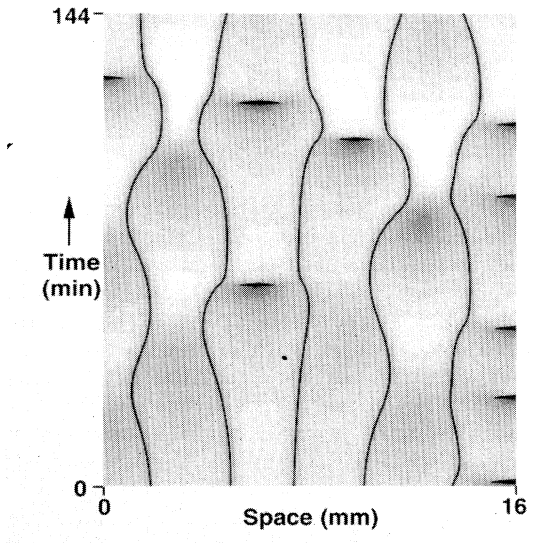

FIG. 24. Oscillating channels with "firings" in numerical simulation. The time asymptotic behavior is shown for $[H^+]_0 = 2.0$ mM. Other parameter values are the same as given in the caption for Fig. 21.

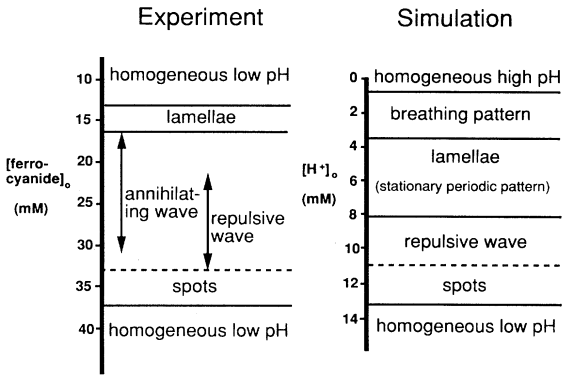

FIG. 25. Bifurcations in the experiments (Sec. IV) and simulations (Sec. V) as a function of $[K_4Fe(CN)_6 \cdot 3H_2O]_0$ and $[H^+]_0$, respectively. Other parameter values are the same as given in the captions for Figs. 11 and 21. The lamellae in these experiments differ from those in the transition sequence in Fig. 10 (see Sec. III); the experimental conditions that differ are the concentration of $[H^+]_0$, which is 9.0 mM for Fig. 10 and 7.2 mM here, and the gel thickness, which is 0.2 mm for Fig. 10 and 0.4 mm here. Also, the total flow rates (varied) used for the experiments of Fig. 10 are higher than those used here (86.4 ml/h).

fine control parameter mesh to search for this type of pattern between the homogeneous and lamellae regimes.

D. Bifurcation diagrams

The result of our experiments (Sec. IV) and one-dimensional simulations of the FIS reaction are summarized in bifurcation diagrams in Fig. 25. No hysteresis was observed in these transitions within the resolution used in the experiment ($\Delta[K_4Fe(CN)_6 \cdot 3H_2O]_0 = 0.8$ mM) and simulation ($\Delta[H^+]_0 = 1.0$ mM). The transition sequences in the experiment and model are similar, but there are differences: the annihilating excitable waves observed in experiment are not found in the numerical study; the complex breathing pattern observed in the simulation (Fig. 24) is not seen in experiment; at low control parameter concentrations, a low (high) pH homogeneous state is reached in the experiment (simulation).

VI. DISCUSSION

A. Lamellae in other model systems

Pattern formation has been extensively studied in recent analyses of amplitude equations [1], but this approach is limited to small amplitude patterns; hence it cannot be used to study large amplitude patterns such as the lamellae and replicating spots. There have been few studies of large amplitude reaction-diffusion patterns other than conventional excitable waves. In 1980, Koga and Kuramoto showed that stable large amplitude lo-

calized patterns could form in a Bonhoeffer–van der Pol model system both in monostable and bistable regimes [37]. This analysis of a one-dimensional system was extended to two dimensions by Otha *et al.*, who reduced the original system to an interface equation governing the boundary separating "high" and "low" states [38]. They studied different types of instabilities of an isolated disk and a band structure, but they did not find space filling patterns such as the lamellae we have described.

Our observations of lamellar patterns motivated Pearson to conduct a numerical study of a Gray-Scott model [39]. He found not only lamellae that are similar to those observed in our experiments on the FIS reaction, but also other patterns. Subsequently, Petrich and Goldstein obtained a similar lamellar structure in a numerical study of the dynamics of an interface [40], an approach similar to that of Otha *et al.* [38]. The equation governing the interfacial dynamics was obtained by taking a singular limit of the FitzHugh-Nagumo model. The resulting model is variational; the final state minimizes the free energy of the system. Another variational system was studied by Frisch *et al.* [41]. Numerical simulation of a Swift-Hohenberg equation with a constant flux term revealed stationary lamellae and a bifurcation diagram similar to that obtained in our experiments (Fig. 11).

Hagberg and Meron [35,42–44] have gained insights into lamellar patterns from an analysis of the Ising-Bloch transition and the transverse instability of the front. At an Ising-Bloch transition, a state initially supporting propagating fronts with a single speed (v; the Ising regime) undergoes a transition to a state supporting two counterpropagating fronts with two different speeds (u and u'; Bloch regime). Beyond the transverse instability a flat front that was formerly stable becomes unstable to small fluctuations. Hagberg and Meron find that in the Ising regime, lamellae arise due to a transverse instability. Far inside the Ising regime, the system can be reduced to a variational system using a singular perturbation method. In this analysis lamellae can form in both nonvariational and variational regimes; therefore, nonvariational effects are not crucial for the formation of lamellae.

The models that have been found to yield lamellae all have cubic nonlinearities and have an inhibitor species that diffuses faster than the activator. These observations are consistent with an analysis conducted by Horvath *et al.* [45], who found that the transverse front instability, which is essential for the formation of lamellae, can occur only if the system has a cubic nonlinearity (a quadratic term alone is insufficient) and if the inhibitor diffuses faster than the activator.

It is difficult to make a direct comparison between the two-variable model systems and the more realistic four-variable FIS system we have analyzed. However, an effective cubic nonlinearity can be obtained in the FIS system by combining two of the five kinetic equations ($2Y \rightarrow Z$, $Z+X \rightarrow 3Y$) to obtain ($2Y+X \rightarrow 3Y$) with a cubic nonlinearity. The simulations of the FIS model that we have described were conducted with $D_X = 2D_Y$ [46]. Simulations with $D_Y > D_X$ did not yield stationary lamellae, which seems consistent with the requirement of faster diffusion of the inhibitor species. However, the situation is unclear because H^+ diffuses faster than other reaction components.

B. Understanding spot replication

Insight into spot replication has been achieved by Pearson and collaborators [24,39,47] from a simulation of the Gray-Scott model. In this model a spot is a region of high V (activator) and low U (inhibitor). The spot is maintained by the diffusive flux of U (the more rapidly diffusing species) through the boundary of spot and from the reservoir, where the concentrations of U and V are kept at 1 and 0, respectively. Inside the spot, U is constantly consumed in producing V through a catalytic reaction $U + 2V \rightarrow 3V$, while in the spot V decreases through diffusion into the reservoir and the spot's surroundings. Whether a spot grows or shrinks depends on the magnitude of the flux of U, F_c, above (below) which the boundary moves toward the region of higher (lower) U.

If an expanding spot interacts with neighboring spots, it does not grow isotropically and the local curvature along the spot boundary varies. As the curvature decreases, F becomes smaller than F_c first in the portion of minimum curvature, at which point a portion of the boundary retreats instead of expanding and replication occurs, as shown in Fig. 11(a).

Spots repel when they approach close to one another because the region between them becomes depleted in U and cannot support the high V state. If spots become overcrowded, many of them die. The flux of U into a surviving isolated spot is almost isotropic and the spot expands until the flux of U is insufficient to maintain the spot center in the high V state. Then the center collapses, leaving an annular ring, as shown in Fig. 11(b). These annular structures eventually break into pieces through interactions with neighbors.

This explanation of spot division is consistent with a recent analysis by Meron and his co-workers of a FitzHugh-Nagumo model [43,44]. They find that the dynamics of chemical front depends strongly on the concentration of the inhibitor species at the chemical front; similarly, in the description given above, the front dynamics depends on the flux of the inhibitor at the front. Replicating spots are found near the Ising-Bloch bifurcation in the Ising regime, where dynamic front transitions can be induced by curvature variations. In this regime, the velocity-curvature relation is multivalued: there are two stable solution branches corresponding to two counterpropagating fronts. The transitions between two solution branches can occur when the front curvature falls below $K_{\min}$ or exceeds $K_{\max}$. The pinching of a spot corresponds to a retreat of a portion of boundary at $K_{\min}$, while the other parts of the front are still expanding. Similarly, $K_{\max}$ corresponds to a minimum spot size, at which point a spot will stop shrinking and begin to grow. Measurements of the critical radii in our experiment yield $(K_{\min})^{-1} = 4.3$ mm and $(K_{\max})^{-1} = 0.6$ mm for the conditions given in the caption of Fig. 11.

C. Other related work

In experiments on a chlorite-iodide-malonic acid reaction, De Kepper *et al.* recently observed a "cell splitting" growth mechanism which leads to a stationary pattern [14]. The relation between the dynamic replicating spot patterns that we observed and the transient splitting phenomenon found by De Kepper *et al.* should be the subject of a future study.

Middya and Luss have studied the effects of coupling between the reaction in the reservoir and that in the gel [48]. Numerical simulations on a Gray-Scott model showed that the patterns can be qualitatively changed if the global coupling is sufficiently strong. In another study with strong global coupling, Krischer and Mikhailov found that there is a bifurcation to traveling spots [49]. However, the global coupling is fairly weak for the conditions of our experiments since the gel volume (≤ 0.2 ml) is much smaller than the reservoir volume.

Self-replication of pulses in a superconductor was found more than a decade ago by Akmetov and Mints [50], who studied a model system consisting of three coupled partial differential equations with two time scales. Self-replication of superconducting pulses was subsequently found in experiments (see the discussion in [51]). The phenomena in superconductors and reaction-diffusion systems appear to be quite similar.

D. Concluding remarks

The lamellae and replicating spots that we have observed in a ferrocyanide-iodate-sulfite reaction are different from the patterns previously observed in chemical systems. The discovery of similar patterns in several different reaction-diffusion models suggests that there is nothing remarkable about the FIS reaction—lamellae and replicating spots can be expected to form in other chemical systems. Similarly, small amplitude Turing patterns may form in the FIS system under suitable conditions. Clearly there is a need for laboratory and theoretical studies of other reactions. Studies of homogeneous chemical reactions in stirred flow reactors have established models for the kinetics of several reactions that exhibit bistability and oscillations. Such reactions would be good candidates for future laboratory experiments on pattern formation and for numerical studies of two and three-dimensional reaction-diffusion models.

ACKNOWLEDGMENTS

We acknowledge fruitful discussions with M. Florian, G. H. Gunaratne, A. Lee, E. Meron, Q. Ouyang, J. E. Pearson, and especially with W. D. McCormick. This work was supported by the U.S. Department of Energy Office of Basic Energy Sciences and the Robert A. Welch Foundation.

[1] M. C. Cross and P. C. Hohenberg, Rev. Mod. Phys. **65**, 851 (1993).
[2] A. M. Turing, Philos. Trans. R. Soc. London Ser. B **327**, 37 (1952).
[3] H. Meinhardt, *Models of Biological Pattern Formation* (Academic, New York, 1986).
[4] J. D. Murray, *Mathematical Biology* (Springer-Verlag, New York, 1989).
[5] L. G. Harrison, *Kinetic Theory of Living Pattern* (Cambridge University Press, New York, 1993).
[6] Z. Noszticzius, W. Horsthemke, W. D. McCormick, and H. L. Swinney, Nature **329**, 6140 (1987).
[7] W. Y. Tam, W. Horsthemke, W. D. McCormick, and H. L. Swinney, U.S. Patent, No. 4,832,914 (23 May 1989); Z. Noszticzius, W. Horsthemke, W. D. McCormick, H. L. Swinney, and W. Y. Tam, U.S. Patent, No. 4,968,484 (6 November 1990).
[8] W. Y. Tam, W. Horsthemke, Z. Noszticzius, and H. L. Swinney, J. Chem. Phys. **88**, 3395 (1988).
[9] G. S. Skinner and H. L. Swinney, Physica D **48**, 1 (1991).
[10] V. Castets, E. Dulos, J. Boissonade, and P. De Kepper, Phys. Rev. Lett. **64**, 2953 (1990); P. De Kepper, V. Castets, E. Dulos, and J. Boissonade, Physica D **49**, 161 (1991); J. Boissonade, V. Castets, E. Dulos, and P. De Kepper, in *Bifurcation and Chaos: Analysis, Algorithms, and Applications*, edited by T. Küpper, F. W. Schneider, R. Seydel, and H. Troger, International Series of Numerical Mathematics Vol. 97 (Birkhäuser, Basel, 1991), p. 67; K. Agladze, E. Dulos, and P. De Kepper, J. Phys. Chem. **96**, 2400 (1992); J. Boissonade, E. Delos, and P. De Kepper, in *Chemical Waves and Patterns*, edited by R. Kapral and K. Showalter (Kluwer, Dordrecht, 1995).
[11] Q. Ouyang and H. L. Swinney, Nature **352**, 610 (1991); K. J. Lee, W. D. McCormick, Z. Noszticzius, and H. L. Swinney, J. Chem. Phys. **96**, 4048 (1992); Z. Noszticzius, Q. Ouyang, W. D. McCormick, and H. L. Swinney, J. Phys. Chem. **96**, 6303 (1992); Q. Ouyang, G. H. Gunaratne, and H. L. Swinney, Chaos **3**, 4 (1993); Q. Ouyang and H. L. Swinney, in *Chemical Waves and Patterns* (Ref. [10]); G. H. Gunaratne, Q. Ouyang, and H. L. Swinney, Phy. Rev. E **50**, 2802 (1994).
[12] I. Lengyel and I. R. Epstein, Science **251**, 650 (1991); I. Lengyel, S. Kádár, and I. R. Epstein, Phys. Rev. Lett. **69**, 2729 (1992).
[13] J. J. Perraud, K. Agladze, E. Dulos, and P. De Kepper, Physica A **188**, 1 (1992); J. J. Perraud, A. De Wit, E. Dulos, P. De Kepper, G. Dewel, and P. Borckmans, Phys. Rev. Lett. **71**, 1272 (1993).
[14] P. De Kepper, J. J. Perraud, D. Rudovics, and E. Dulos, Int. J. Bif. Chaos **4**, 1215 (1994).
[15] Q. Ouyang and H. L. Swinney, Chaos **1**, 4 (1991).
[16] E. C. Edblom, M. Orbán, and I. R. Epstein, J. Am. Chem. Soc. **108**, 2826 (1986).
[17] E. C. Edblom, L. Gyorgyi, and I. R. Epstein, J. Am. Chem. Soc. **109**, 4876 (1987).
[18] V. Gáspár and K. Showalter, J. Am. Chem. Soc. **109**, 4869 (1987).
[19] V. Gáspár and K. Showalter, J. Phys. Chem. **94**, 4973 (1990).
[20] K. J. Lee, W. D. McCormick, Q. Ouyang, and H. L. Swinney, Science **261**, 192 (1993).
[21] G. Nicolis and I. Prigogine, *Self-Organization in Nonequi-*

librium Chemical Systems (Wiley, New York, 1977).
[22] Y. Kuramoto, *Chemical Oscillations, Waves, and Turbulence* (Springer-Verlag, Berlin, 1984).
[23] J. E. Pearson and W. Horsthemke, J. Chem. Phys. **90**, 1588 (1989); J. E. Pearson and W. J. Bruno, Chaos **2**, 513 (1992).
[24] K. J. Lee, W. D. McCormick, J. E. Pearson, and H. L. Swinney, Nature **369**, 215 (1994).
[25] The gel membranes used in the experiments in Secs. III and IV are 0.2 and 0.4 mm thick, respectively. The thicker membrane was used because it was stronger and easier to handle. The residence time of the reactants depends on gel thickness; hence the reservoir concentrations that yield any given pattern depend on gel thickness.
[26] References [20,24] incorrectly stated that ferrocyanide is the species that absorbs light at 420 nm. As Fig. 3(b) shows, ferricyanide is the principal species that absorbs light at 420 nm.
[27] In our earlier work [20,24], most patterns were visualized using bromothymol blue indicator; hence low *p*H regions were white and high *p*H regions black. To minimize confusion related simply to the technique of visualizing the patterns, all patterns in [20,24] were presented with low *p*H regions in white and high *p*H regions in black, regardless of the visualization technique. The opposite convention is used in the present paper where most of the data were obtained in observations at 420 nm without using a *p*H indicator.
[28] A. N. Zakin and A. M. Zhabotinsky, Nature **225**, 535 (1970); A. T. Winfree, Science **175**, 634 (1972); P. Foerster, S. Müller, and B. Hess, *ibid.* **241**, 685 (1988); J. Maselko and K. Showalter, Nature **339**, 22 (1989).
[29] A. M. Zhabotinsky, M. D. Eager, and I. R. Epstein, Phys. Rev. Lett. **71**, 1526 (1993).
[30] P. Gray and S. K. Scott, Ber. Bunsenges. Phys. Chem. **90**, 985 (1986).
[31] B. Peng, V. Gáspár, and K. Showalter, Philos. Trans. R. Soc. London Ser. A **337**, 275 (1991).
[32] Y. Luo and I. R. Epstein, J. Phys. Chem. **93**, 1398 (1989).
[33] The parameter k_0 is closely related to the parameter F (total input flow rate to the reactor reservoir) used in the experiments: as F increases, the chemical concentrations in the reservoir increase and the flux exchange terms (terms with k_0 in the model) change accordingly since they depend on the differences in chemical concentrations between the gel and the reservoir. However, a direct comparison between F and k_0 would require a three-dimensional simulation of the gel reaction-diffusion system.
[34] I. F. Shampine and H. A. Watts, Sandia Laboratories Report No. SAND79-2374 (unpublished).
[35] A. Hagberg and E. Meron, Nonlinearity **7**, 805 (1994).
[36] C. Misbah and A. Valance, Phys. Rev. E **49**, 166 (1994).
[37] S. Koga and Y. Kuramoto, Prog. Theor. Phys. **63**, 106 (1980).
[38] T. Otha, M. Mimura, and R. Kobayashi, Physica D **34**, 115 (1989).
[39] J. E. Pearson, Science **261**, 189 (1993).
[40] D. M. Petrich and R. E. Goldstein, Phys. Rev. Lett. **72**, 1120 (1994).
[41] T. Frisch, A. C. Newell, and T. Passot (unpublished).
[42] A. Hagberg and E. Meron, Phys. Rev. Lett. **72**, 2494 (1994).
[43] C. Elphick, A. Hagberg, and E. Meron, Phys. Rev. E (to be published).
[44] A. Hagberg and E. Meron, Chaos **4**, 477 (1994).
[45] D. Horváth, V. Petrov, S. Scott, and K. Showalter, J. Chem. Phys. **98**, 6332 (1993); see also Z. Zhang and S. A. E. Falle, Proc. R. Soc. London Ser. A **446**, 1 (1994).
[46] In a two-variable model obtained from a reduction of the four-variable model we have used, X and Y are, respectively, the inhibitor and the activator [19].
[47] W. N. Reynolds, J. E. Pearson, and S. Ponce-Dawson, Phys. Rev. Lett. **72**, 2794 (1994).
[48] U. Middya and D. Luss, J. Chem. Phys. **100**, 6386 (1994).
[49] K. Krischer and A. Mikhailov, Phys. Rev. Lett. **73**, 3165 (1994).
[50] A. A. Akhmetov and R. G. Mints, J. Phys. D **16**, 2505 (1983); V. S. Kovner and R. G. Mints, J. Appl. Phys. **75**, 7538 (1994).
[51] A. V. Gurevich and R. G. Mints, Rev. Mod. Phys. **59**, 941 (1987).

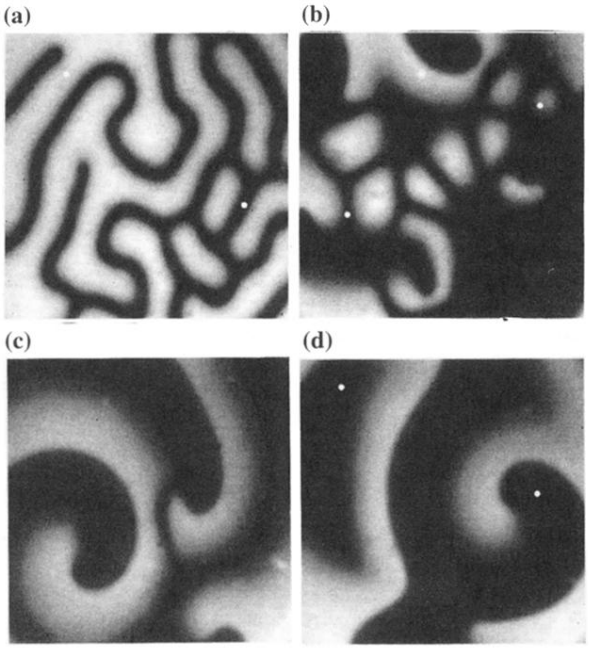

FIG. 1. Patterns observed in experiments with different ferrocyanide concentrations in the feed: (a) lamellae; (b) self-replicating spots; (c) spiral waves with wave front repulsion; (d) spiral waves with wave front annihilation. The patterns are illuminated in the blue (400–440 nm) and shown in full gray scale. The low pH state (roughly pH 4), which absorbs strongly in the blue, appears black, while the high pH state (roughly pH 7), appears white. The small white circles are end points of lines showing one-dimensional intensity profiles in Fig. 8. Each domain is 16×16 mm^2. The ferrocyanide concentrations in the feed are (in mM): $[K_4Fe(CN)_6{\cdot}3H_2O]_0$ = 14.2, 36.4, 30.0, and 25.0, respectively for (a)–(d). The concentrations of other reagents fed into the reservoir are held fixed (in mM): $[NaIO_3]_0$ = 75.0, $[Na_2SO_3]_0$ = 89.0, $[H_2SO_4]_0$ = 3.6, and $[NaOH]_0$ = 0.25, where the 0 subscript denotes values in the reservoir. The total input flow rate is 86.4 ml/h and the thickness of polyacrylamide gel is 0.4 mm.

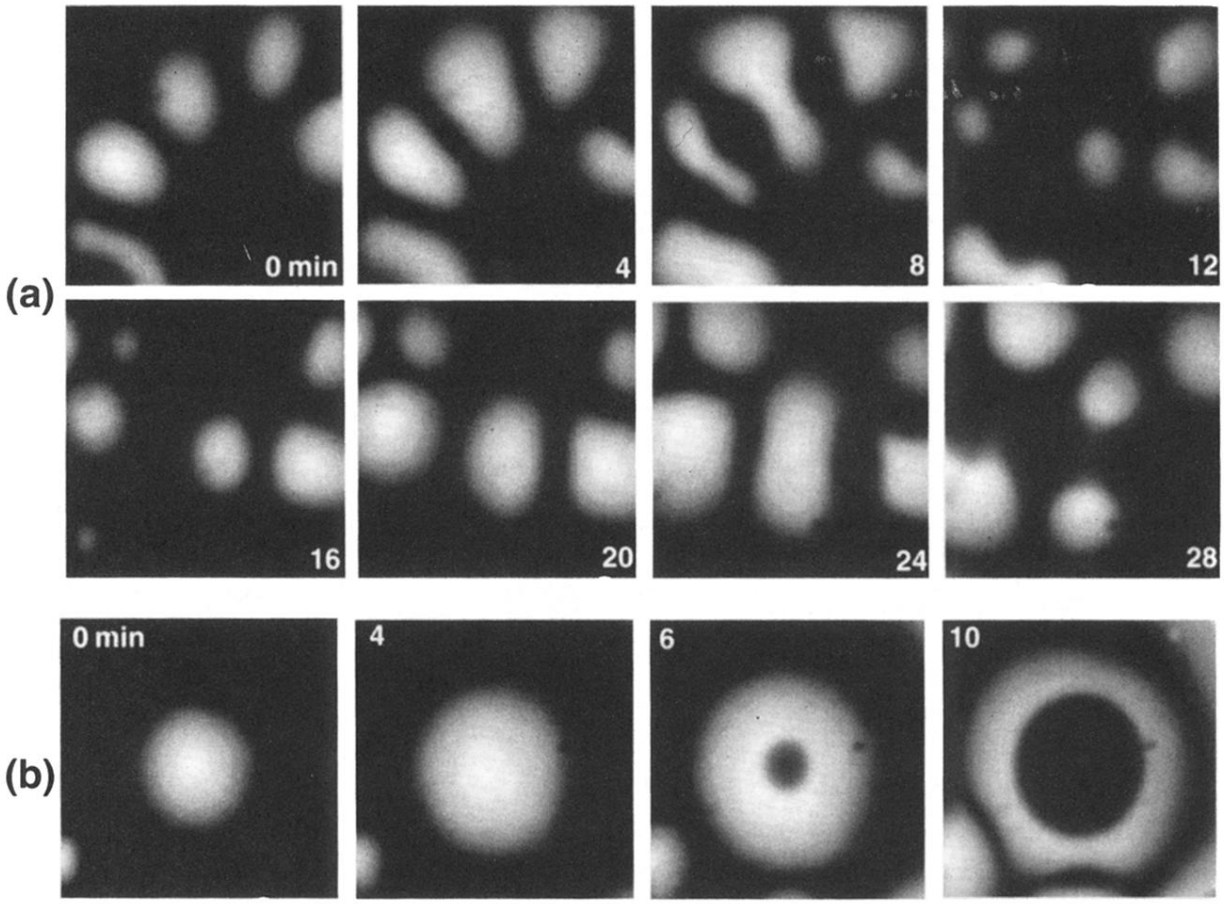

FIG. 11. Experimental observations of (a) self-replicating spots and (b) formation of a ring. In (a), chemical spots (white; high pH) undergo two successive divisions. The divisions are strongly influenced by neighboring spots. Each frame is 7×7 mm^2. In (b), an isolated spot of high pH state grows until its center collapses into the low pH state. The ring eventually interacts with neighboring structures and breaks. Each frame is 10×10 mm^2. Both (a) and (b) are observed with illumination at 420 nm in a system without bromothymol blue indicator. Both phenomena are observed with following parameter values: $[K_4Fe(CN)_6{\cdot}3H_2O]_0 = 36.4$ mM, $[NaIO_3]_0 = 75.0$ mM, $[Na_2SO_3]_0 = 89.0$ mM, $[H_2SO_4]_0 = 3.6$ mM, and $[NaOH]_0 = 0.25$ mM. The total input flow rate is 86.4 ml/h and the thickness of the gel membrane is 0.4 mm.

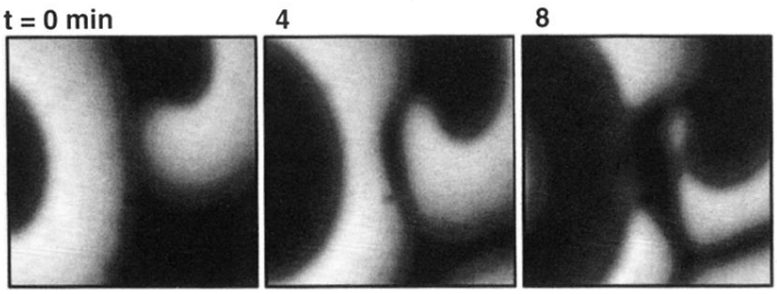

FIG. 13. Snapshots showing a repulsive chemical front interaction. The patterns are observed in illumination at 420 nm without bromothymol blue indicator. The domain is 8.2×8.2 mm^2. The parameter values are the same as given in the caption for Fig. 11, except $[K_4Fe(CN)_6 \cdot 3H_2O]_0 = 30.0$ mM.

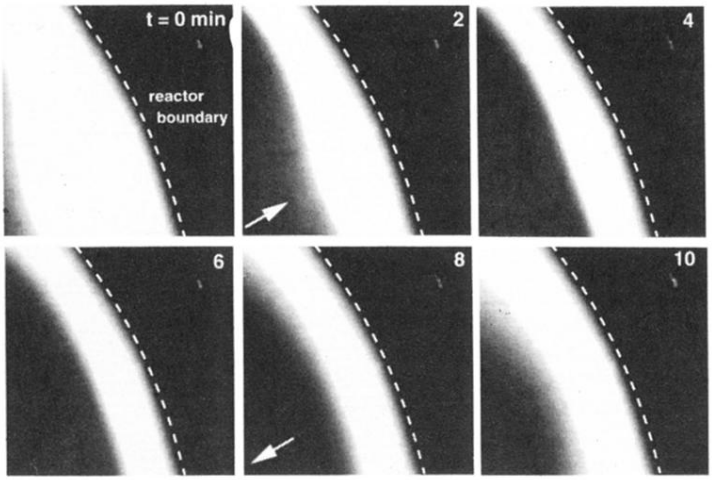

FIG. 14. Snapshots showing observations of an excitable wave reflecting from the reactor boundary. The patterns are observed in illumination at 420 nm without bromothymol blue indicator. The domain is 5.2×5.2 mm^2. The parameter values are the same as given in the caption for Fig. 13.

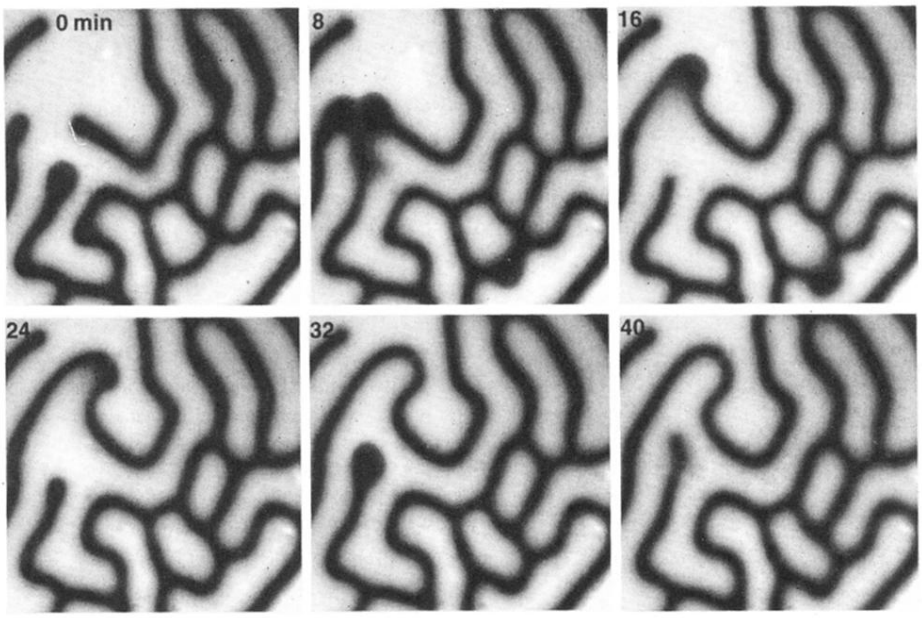

FIG. 15. Snapshots of a pattern evolving to a stationary pattern of low pH lamellae in a high pH background. Unlike the lamellar pattern in a bistable regime (Fig. 5), the fronts sometimes collide and annihilate. The patterns are observed in illumination at 420 nm without bromothymol blue indicator. The domain is 16 $\times$ 16 mm^2. The parameter values are the same as given in the caption for Fig. 11, except $[K_4Fe(CN)_6{\cdot}3H_2O]_0 = 14.2$ mM.

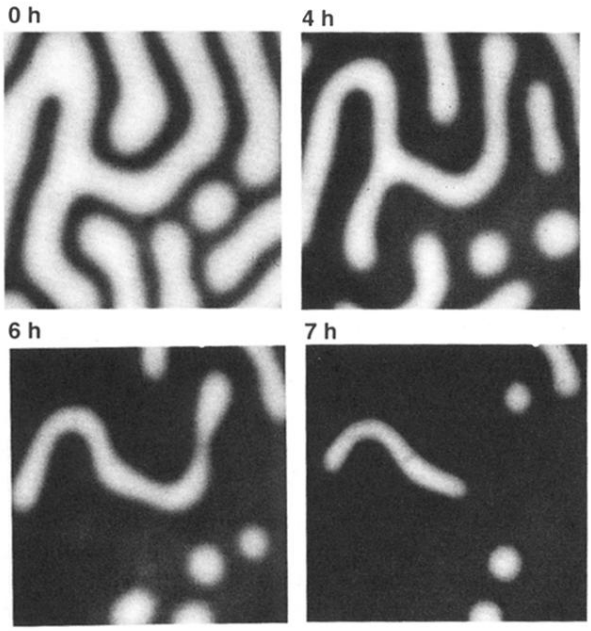

FIG. 16. Transition from a lamellar pattern to the homogeneous low pH state, observed following a decrease in $[K_4Fe(CN)_6 \cdot 3H_2O]_0$ from 14.2 mM to 13.0 mM at $t = 0$. The high pH stripes disappear more by shrinking in length than by decreasing in thickness. The patterns are observed in illumination at 420 nm without bromothymol blue indicator. The domain is 13×13 mm^2. Other parameter values are held fixed as given in Fig. 11.

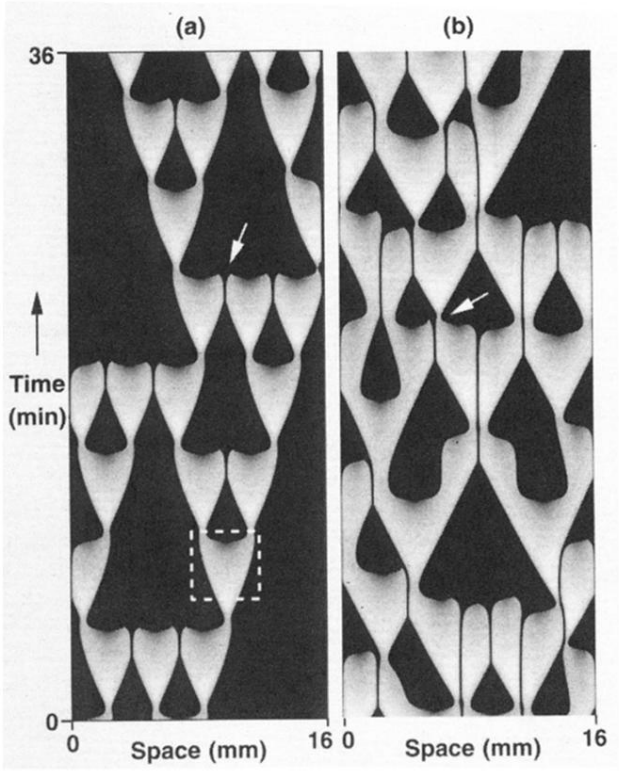

FIG. 21. Numerical simulations of (a) one-dimensional replicating spots and (b) excitable waves with front repulsions. Both space-time diagrams show asymptotic behavior after initial transients have decayed. A small domain of high pH (pH 8; white) is seeded initially as a perturbation of a homogeneous low pH (pH 3; black) state (not shown in the figure) and subsequent time evolution is integrated. In (b) the interaction of fronts and the reflection from walls are similar to that in the laboratory observations shown in Figs. 13 and 14. The parameter values used in (a) are $[Fe(CN)_6{}^{-4}]_0 = 2.5$ mM, $[IO_3{}^-]_0 = 75.0$ mM, $[H^+]_0 = 12.5$ mM, $[SO_3{}^{-2}]_0 = 89.3$ mM, and $k_0 = 1.0 \times 10^{-4}$ s^{-1}. The parameter values for (b) are the same as in (a), except that $[H^+]_0 = 11.0$ mM.

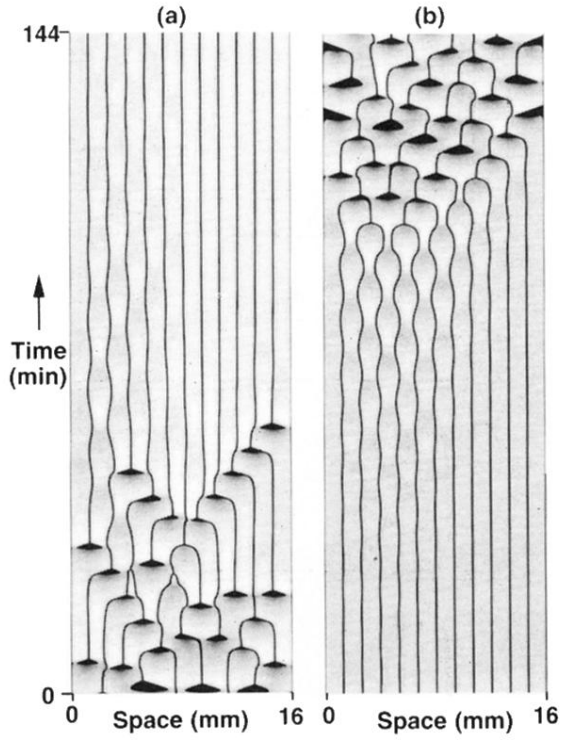

FIG. 23. (a) Space-time evolution showing formation of a stationary periodic structure in numerical simulation, after $[H^+]_0$ is decreased from 8.5 mM, where waves repel and there is no asymptotic stationary pattern, to $[H^+]_0 = 7.5$ mM, where the pattern stabilizes in a stationary spatially periodic structure. The transient behavior, although one dimensional, has similarities to that observed in experiments on two-dimensional patterns (Fig. 15). (b) Destabilization of a stationary structure. $[H^+]_0$ is increased from 7.5 mM to 8.5 mM at $t = 0$. Other parameter values are held fixed as given in the caption for Fig. 21.

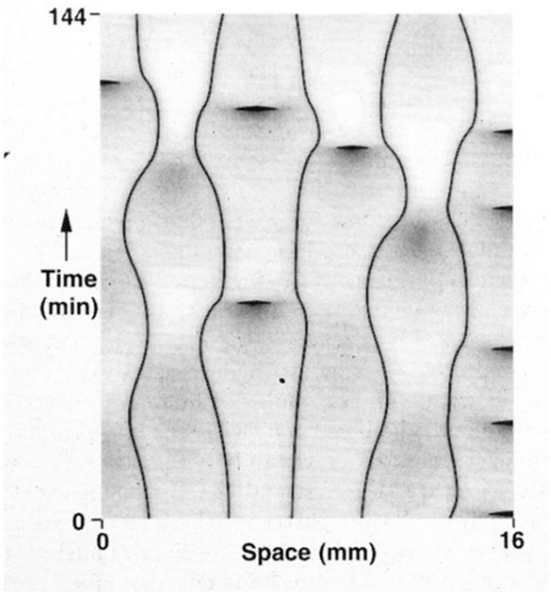

FIG. 24. Oscillating channels with "firings" in numerical simulation. The time asymptotic behavior is shown for $[H^+]_0 = 2.0$ mM. Other parameter values are the same as given in the caption for Fig. 21.

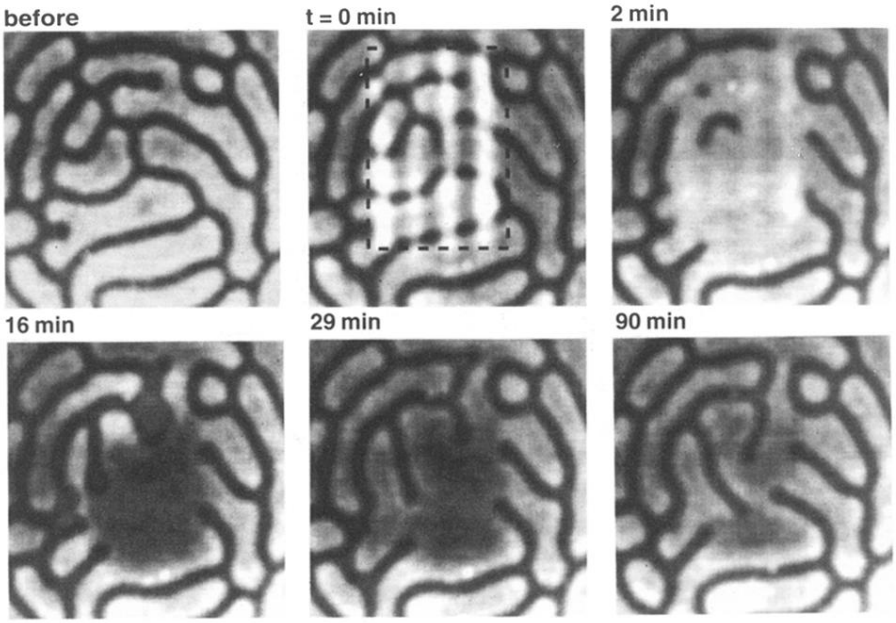

FIG. 7. Time evolution of lamellae following a perturbation with ultraviolet light. The perturbation is made with a striped mask for 5 minutes; only the boxed region bounded by dashed lines is perturbed. The perturbation is removed at $t = 0$. The patterns are observed with bromothymol blue indicator in reflected light of 620 nm (but note that black corresponds to low pH and white to high ph; see the caption to Fig. 5). Each frame is 13×13 mm^2. The parameter values are the same as given in the caption for Fig. 5.